AIP | Journal of Applied Physics

Mechanisms of boron diffusion in silicon and germanium

S. Mirabella, D. De Salvador, E. Napolitani, E. Bruno, and F. Priolo

Citation: J. Appl. Phys. **113**, 031101 (2013); doi: 10.1063/1.4763353
View online: http://dx.doi.org/10.1063/1.4763353
View Table of Contents: http://jap.aip.org/resource/1/JAPIAU/v113/i3
Published by the American Institute of Physics.

Related Articles

A model for phosphosilicate glass deposition via POCl3 for control of phosphorus dose in Si
J. Appl. Phys. 112, 124912 (2012)

Effect of near atmospheric pressure nitrogen plasma treatment on Pt/ZnO interface
J. Appl. Phys. 112, 116104 (2012)

Observation of boron diffusion in an annealed Ta/CoFeB/MgO magnetic tunnel junction with standing-wave hard x-ray photoemission
Appl. Phys. Lett. 101, 202402 (2012)

An all optical mapping of the strain field in GaAsN/GaAsN:H wires
Appl. Phys. Lett. 101, 191908 (2012)

Note: Effective diffusion coefficient in heterogeneous media
J. Chem. Phys. 137, 166101 (2012)

Additional information on J. Appl. Phys.

Journal Homepage: http://jap.aip.org/
Journal Information: http://jap.aip.org/about/about_the_journal
Top downloads: http://jap.aip.org/features/most_downloaded
Information for Authors: http://jap.aip.org/authors

ADVERTISEMENT

JOURNAL OF APPLIED PHYSICS 113, 031101 (2013)

APPLIED PHYSICS REVIEWS—FOCUSED REVIEW

Mechanisms of boron diffusion in silicon and germanium

S. Mirabella,[1,a)] D. De Salvador,[2] E. Napolitani,[2] E. Bruno,[1] and F. Priolo[1]
[1]*MATIS IMM-CNR and Dipartimento di Fisica e Astronomia, Università di Catania, Via Santa, Sofia 64, Catania I-95123, Italy*
[2]*MATIS IMM-CNR and Dipartimento di Fisica e Astronomia, Università di Padova, Via, Marzolo 8, Padova I-35131, Italy*

(Received 13 June 2012; accepted 25 September 2012; published online 16 January 2013)

B migration in Si and Ge matrices raised a vast attention because of its influence on the production of confined, highly *p*-doped regions, as required by the miniaturization trend. In this scenario, the diffusion of B atoms can take place under severe conditions, often concomitant, such as very large concentration gradients, non-equilibrium point defect density, amorphous-crystalline transition, extrinsic doping level, co-doping, B clusters formation and dissolution, ultra-short high-temperature annealing. In this paper, we review a large amount of experimental work and present our current understanding of the B diffusion mechanism, disentangling concomitant effects and describing the underlying physics. Whatever the matrix, B migration in amorphous (α-) or crystalline (c-) Si, or c-Ge is revealed to be an indirect process, activated by point defects of the hosting medium. In α-Si in the 450-650 °C range, B diffusivity is 5 orders of magnitude higher than in c-Si, with a transient longer than the typical amorphous relaxation time. A quick B precipitation is also evidenced for concentrations larger than 2×10^{20} B/cm^3. B migration in α-Si occurs with the creation of a metastable mobile B, jumping between adjacent sites, stimulated by dangling bonds of α-Si whose density is enhanced by B itself (larger B density causes higher B diffusivity). Similar activation energies for migration of B atoms (3.0 eV) and of dangling bonds (2.6 eV) have been extracted. In c-Si, B diffusion is largely affected by the Fermi level position, occurring through the interaction between the negatively charged substitutional B and a self-interstitial (*I*) in the neutral or doubly positively charged state, if under intrinsic or extrinsic (*p*-type doping) conditions, respectively. After charge exchanges, the migrating, uncharged B*I* pair is formed. Under high *n*-type doping conditions, B diffusion occurs also through the negatively charged B*I* pair, even if the migration is depressed by Coulomb pairing with *n*-type dopants. The interplay between B clustering and migration is also modeled, since B diffusion is greatly affected by precipitation. Small (below 1 nm) and relatively large (5-10 nm in size) B*I* clusters have been identified with different energy barriers for thermal dissolution (3.6 or 4.8 eV, respectively). In c-Ge, B motion is by far less evident than in c-Si, even if the migration mechanism is revealed to be similarly assisted by *I*s. If *I*s density is increased well above the equilibrium (as during ion irradiation), B diffusion occurs up to quite large extents and also at relatively low temperatures, disclosing the underlying mechanism. The lower B diffusivity and the larger activation barrier (4.65 eV, rather than 3.45 eV in c-Si) can be explained by the intrinsic shortage of *I*s in Ge and by their large formation energy. B diffusion can be strongly enhanced with a proper point defect engineering, as achieved with embedded GeO_2 nanoclusters, causing at 650 °C a large *I*s supersaturation. These aspects of B diffusion are presented and discussed, modeling the key role of point defects in the two different matrices. © *2013 American Institute of Physics*. [http://dx.doi.org/10.1063/1.4763353]

TABLE OF CONTENTS

I. INTRODUCTION 2
II. B DIFFUSION IN α-SI: THE MEDIATION OF DANGLING BONDS 3
A. Defects and diffusion in amorphous Si 3
B. Main features of B migration 4
C. Defect assisted B diffusion 6
III. B DIFFUSION IN c-Si: ATOMISTIC MECHANISM, ENERGETICS AND CLUSTERING. 7
A. Milestones on the B diffusion mechanism. . 7
B. Atomistic pathways of B diffusion 9
C. Energetics of B diffusion 11

a)Author to whom correspondence should be addressed. Electronic mail: mirabella@ct.infn.it.

 © 2013 American Institute of Physics

D. B-*I* clusters formation and dissolution 12
IV. B DIFFUSION IN c-Ge: THE ROLE OF SELF-INTERSTITIALS. 15
A. B doping in Ge 15
B. Out of equilibrium approach for B migration study. 16
C. Point defect engineering and enhanced B diffusion 18
V. CONCLUSIONS. 19

I. INTRODUCTION

The diffusion of B atoms in silicon represents an emblematic issue for the indirect migration process of impurities in solid materials, as it is well-established that B diffuses in crystalline Si (c-Si) mainly through the interaction with self-interstitial Si atoms (*Is*).[1–4] Such a phenomenon is nowadays largely understood and quite precisely modeled as it has been studied for more than four decades by the material science community. Actually, it is both an exciting solid-state physics issue, due to the relevant underlying microscopic mechanisms, and a continuous challenging topic, because of the noteworthy applications in miniaturized microelectronics devices (B being the main *p*-type dopant in Si). Nonetheless, B diffusion is still studied since next technological designs scheduled by the International Technology Roadmap for Semiconductors (ITRS),[5] such as the sub-22 nm nodes, require dopant diffusion to be controlled down to or even below the nanometer scale and, what is more constraining, under really severe processing conditions.

The miniaturization trend has driven great efforts for developing advanced processing recipes, involving refined combination of sophisticated techniques among which pre-amorphization implant (PAI), sub-1 keV B implantation, millisecond flash and/or laser annealing, C or F co-implantation, and cluster B implantation.[6–9] Under such extreme conditions, the diffusion of B occurs with features that need to be detailed and modeled. Just to appreciate the effect of some post-implantation annealing recipes (750 °C-15 min, 1000 °C spike, and 1300 °C single or multiple flash anneals), in Fig. 1, boron chemical profiles are shown for pre-amorphized Si implanted with 0.5 keV, 1×10^{15} B^+/cm^2.[6] Significant differences both in the diffused profiles and in the B activation levels were evidenced, due to the interplay with the concomitant thermal evolution of the extended defects created by the PAI and of the clustered B. In fact, for the higher temperature anneals, B profiles show a clear immobile peak (indicated by the arrows) due to B precipitation, not visible at 750 °C because of the low B diffusivity.[6] For low thermal budget, a less effective defect dissolution occurs, determining a lower *Is* density and, as a consequence, a lower boron broadening. The spike or flash anneal gives out a broader final boron profile since larger *Is* emission from extended defects occurs as well as the concomitant B clusters dissolution. On the other hand, B clusters significantly act as independent scattering centers, lowering the hole mobility down to ~40% of its theoretical value.[6] It should be noted

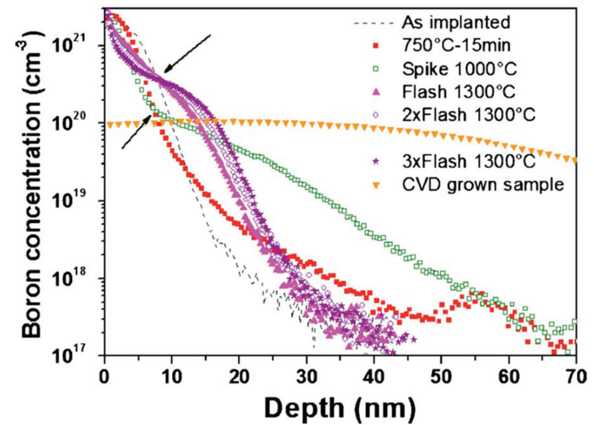

FIG. 1. Chemical profiles SIMS of B atoms after implantation (0.5 keV, $1\times10^{15}/cm^2$) in Ge pre-amorphized Si, and after different thermal processes (750 °C-15 min, 1000 °C spike, 1300 °C single or multiple flash anneals). A boron profile is also reported as a reference sample (grown by chemical vapor deposition, CVD). The kinks (shown by arrows) in the annealed profiles indicate the formation of an immobile B peak (due to B clustering). Reprinted with permission from F. Severac, J. Appl. Phys. **107**, 123711 (2010). Copyright 2010 American Institute of Physics.

that in such extreme conditions, many phenomena actually occur, which heavily affect the diffusion and the electrical activation of boron atoms and, finally, influence the achievement of ultra-shallow and custom-shaped junctions. In order to allow simulation software tools managing the complexity of this last process, a continuous upgrading is needed in the comprehension of the physics underlying all these phenomena, among which the B diffusion and clustering, at very high dopant concentrations, in amorphous Si or in crystalline Si, and, recently, also in Ge lattices.

Typically, B is implanted in silicon previously amorphized by Ge implantation, for avoiding channeling tails and implant damage at the junction depth, while increasing the activation level. Because of this, at the very early stage of annealing and up to the completion of the concomitant solid phase epitaxy regrowth (SPER), B atoms diffuse in the amorphous phase of Si (α-Si) and they typically precipitate into small B clusters, which causes the lack of electrical activation once in the crystalline matrix. Both the diffusion and clustering in α-Si cannot be neglected, since they influence the final B profile and its activation in the desired ultra-shallow junction. In fact, B diffusivity in α-Si is measured to be more than five orders of magnitude larger than in crystalline Si at the same temperature,[10,11] so, even if the SPER can be completed during the rump-up stage of a flash annealing, boron atoms will experience a non negligible diffusion. B diffusion coefficient (D_B) in α-Si, at the temperature of 650 °C and at a concentration level of 1×10^{20} B/cm^3, can be as high as $D_B = 7\times10^{-14}$ cm^2/s, while in c-Si, D_B is about 1×10^{-19} cm^2/s.[11] Moreover, since in α-Si, B diffusivity increases with dopant concentration, a peculiar diffused shape comes out with large shoulders and shortened tails, showing concentration gradients enhanced with respect to the non-diffused profile. Such an effect seems to be opposing the Fick's law, according to which the driving force for migration is the reduction of the concentration slope. Still, in this case, the diffusivity of the migrating species is non

homogeneous at all, depending on the concentration itself.[11] In addition, it was clearly demonstrated that B de-activation is partly due to the dopant clustering in the amorphous phase prior to the completion of the SPER process.[6,12,13] Thus, B migration and precipitation in α-Si need to be detailed, for a complete description of B diffusion.

Once the SPER is complete, the migration of B atoms occurs in the crystalline matrix under extrinsic conditions, because the high dopant concentration at certain temperatures causes the Fermi level shift towards the valence band edge, thus modifying the population of charged *Is* useful for B diffusion. In this condition, the B migration occurs through the interaction with neutral *Is* and also with doubly positively charged *Is*, and the B diffusivity is enhanced by some orders of magnitude with respect to intrinsic conditions. At the temperature of 690 °C, under intrinsic conditions, $D_B = 6 \times 10^{-18}$ cm^2/s, while at the same temperature, if a *p*-type doping at a level of 2.8×10^{19} /cm^3 is present, then D_B increases up to 2×10^{-16} cm^2/s.[14] Also in this case, an apparent violation of the Fick's law occurs as the diffused shape shows concentration gradients, which are larger than in the non-diffused profile, since D_B increases with dopant concentration. In addition, the high B concentration also causes further non-equilibrium precipitation, which adds to clusters generated in amorphous Si. It is straightforward that the formation and dissolution of B clusters affect the dopant diffusion. This still holds not only because B atoms are immobilized and then released but also since these clusters contains Si self-interstitials (needed to start the B migration process), which can be immobilized and released too. Further effects should be considered as the closeness of the surface, and its passivation, the pairing of B with impurities, the formation and dissolution of large *I*-type defects, the presence of new classes of defects,[15] and so on. Thus, it is clear that numerous, simultaneous, and interplaying phenomena affect the B diffusion process and an accurate simulation of B migration should consider all of them at once. In order to achieve a suitable knowledge of the above phenomena, well-designed experiments are needed in which each feature is properly described, disentangling the interaction with other ones. This is just what we want to review here, presenting experimental works aimed at facing in details some aspects of B diffusion and at giving out a model epitomizing each phenomenon.

Recently, a large scientific attention to the B diffusion and activation mechanism in crystalline Ge has also taken place, motivated by the renewed industrial interest due to the low-field carrier mobility higher in Ge than in Si lattice. Moreover, the large compatibility of Ge with the existing Si-based technology has opened the route for the realization of advanced microelectronic devices using Ge. But, even if Ge has been the first semiconductor used in microelectronics, a huge gap still exists between Si and Ge concerning the detailed knowledge and the relative simulation of several phenomena, as dopant diffusion and activation, equilibrium point defects density and diffusion, surface and interface effects, and so on. Actually, in the microelectronic industry, Ge was replaced by Si in the '60 s, and then very few studies have been conducted up to the last decade, when a restored scientific attention focused on many aspects related to its possible application.[16] In particular, quite soon, it has become clear that the B diffusivity in Ge was extremely low,[17] up to 5 orders of magnitude lower than in Si at homologous temperatures,[18] and that a very high electrical activation level can be obtained, well higher than in Si.[19] Because of this, B can be regarded as a good choice as a *p*-type dopant, since it should ensure both precise dopant confinement and high electrical activation. In addition, the low diffusivity of B in Ge raised a significant scientific interest since it is related to the density of intrinsic point defects in Ge and it discloses fascinating similarities with Si in the microscopic migration mechanism.

The present work is divided into three sections, handling the B diffusion process in different matrices. Section II is devoted to the migration mechanism of B into amorphous Si, with a microscopic model enlightening the interplay between B and dangling bonds of the amorphous phase, and the energy barriers involved in the diffusion process. Section III deals with B migration in crystalline Si, studying the atomistic pathways and the energetic of B diffusion under extrinsic conditions, together with the investigation of non-equilibrium formation and dissolution of B clusters. Section IV presents the diffusion mechanism of B in crystalline Ge, in equilibrium and non-equilibrium conditions, evidencing the key role of Ge self-interstitial defects in the B migration process. Finally, in Sec. V, the conclusions are reported with some open points for future investigations.

II. B DIFFUSION IN α-SI: THE MEDIATION OF DANGLING BONDS

A. Defects and diffusion in amorphous Si

Amorphous Si (α-Si) can be prepared with a variety of different techniques, such as vacuum deposition, chemical vapor deposition, laser induced quenching, or amorphization by ion-implantation of c-Si. The structural properties of α-Si, as well as the diffusion of impurities, greatly depend on the synthesis technique. Typically, ion implantation is the preferred methodology to realize α-Si as much similar as possible to the ideal continuous random network of covalently bonded atoms, and, in the following, we will refer to this kind of material, which is the most relevant for microelectronics applications.

In the amorphous phase of non-hydrogenated silicon, the structure of atomic bonding is characterized by a local four-fold coordination with a distortion of the diamond lattice beyond two interatomic distances. The lack of the long-range order (distinctive of the crystalline state) is caused by a quite broad distribution of the Si-Si bong angle (diverging up to 12° from the crystalline value of 109.47°), which leads in the α-Si structure to five- and seven-membered atoms rings in addition to the six-membered atoms rings typical of the diamond lattice.[20,21] The large distribution in the bond angle is due, on one hand, to the distortion of the four-fold coordinated Si atoms from the lattice position and, on the other hand, to the presence of a great amount of coordination defects of α-Si, namely the dangling bond (*db*, a three-fold coordinated Si atom) and the floating bond (*fb*, a five-fold coordinated Si atom).[22–25]

Both the coordination defects and the bond angle distortion depend on the process history of α-Si, since it was widely shown that as-implanted α-Si, if annealed, undergoes a structural relaxation, with a heat release measured by differential scanning calorimetry at temperatures below the onset of crystallization.[26] In the mid nineties, after investigation through Raman spectroscopy, x-ray techniques, and photocarrier lifetime measurements, the origin of this relaxation was attributed to the recombination of the coordination defects, decreasing from ∼0.5% to 0.05%, and to the reduction of the bond angle distortion, from 12° to 9°.[20,27] Such a process was shown to be reversible, even if with an hysteresis loop, since ion implantation (leading to a damage level larger than ∼0.1 displacements per atom) performed on relaxed α-Si reproduces the same strain status as in the as-implanted α-Si.[20,27] High resolution investigation of the radial distribution function of α-Si also showed that the coordination number in the first neighbor atomic shell increases from 3.79 to 3.88 going from the as-implanted to the relaxed state, compatible with the removal of coordination defects during the structural relaxation.[28] This undercoordination in α-Si with respect to four-fold coordinated c-Si was furthermore related to the slightly lower atomic density in α-Si (about 2%) than in c-Si.[28]

The structural relaxation and the defects of α-Si affect the impurity diffusion, as demonstrated by the diffusion investigation on transition metals in α-Si.[29–31] In the relaxed state of α-Si, the diffusivity of metals such as Cu and Pd was found to be 2-5 times higher than in the as-implanted α-Si, where the larger defect density induces temporary trapping phenomena, hampering the migration ability.[30,31] Conversely, theoretical calculations recently showed that the Si self-diffusion in α-Si is enhanced in presence of a high percentage of coordination defects, pointing out that self-diffusion can be assisted by *db* or *fb*.[32] Similarly, B diffusion in α-Si was measured to be larger in the as implanted state than in the relaxed one,[10,11,33] showing peculiar features, such as a transient behavior and a dopant concentration dependence, which will be described in the next paragraph.

The coordination defects of α-Si can enhance or retard the diffusion of impurities or the self-diffusion itself, since they have a central role in the microscopic mechanism of migration. On the other hand, it was shown that the presence of dopants in the structure of α-Si can modify the bonding arrangements.[34–38] By means of x-ray absorption fine structure, photothermal deflection spectroscopy, and electronic transport measurements, Muller *et al.* found that in thermally relaxed α-Si, substitutional dopants (as B, P, As, and Ga) have a strong tendency to enter the Si random network in the form of three-fold coordinated atoms, rather than in the dopant four-fold coordinated site. Moreover, the interconversion towards four-fold coordinated dopant sites should have a large kinetic barrier due to the breaking and rearrangements of a relatively large number of covalent bonds in the vicinity of the dopant atom.[37] Thus, while in c-Si, the ground state for substitutional dopants is the four-fold coordinated site (which is electrically active), in α-Si dopants show the natural, three-fold coordinated, bonding arrangement. Such a change in the coordination number of dopant impurities can have significant effects on the coordination defects of α-Si, especially when the dopant concentration is quite high, as we will see in the following paragraphs regarding B diffusion.

B. Main features of B migration

One of the first evidence of B diffusion in α-Si was given by Jacques *et al.* in ultra-low energy (0.5 keV) B implanted preamorphized Si enriched with fluorine and annealed at 550 °C,[39] showing the formation of a large shoulder in the B profile at the concentration range of 5×10^{18}–1×10^{20} B/cm^3. Later on, the role of fluorine was ruled out by Ray Duffy *et al.*, evidencing how during low temperature annealing (500-600 °C) B diffusion occurs also in F-free α-Si up to very high B concentrations (2×10^{20} at./cm^3), at least two orders of magnitude higher than the mobile boron concentration in c-Si at the same temperatures (Fig. 2).[33] The immobile portion of the B profile (above 2×10^{20} B/cm^3) was attributed to B clustering in α-Si. Actually, the formation of B-B pairs during the very early stages of annealing at 550 °C, while B is still in the amorphous phase of Si, has been evidenced by x-ray absorption near-edge spectroscopy measurements of p^+/n ultrashallow junctions realized by solid-phase epitaxy.[13] The clustered B, formed in α-Si, is then transferred to the c-Si once the SPER is complete, being responsible for the B deactivation measured in the final device.

It should be noted that the B diffused profile (Fig. 2) shows a concentration gradient essentially unaffected with respect to the starting profile, revealing a diffusion mechanism not obeying the Fick's laws. Venezia *et al.* investigated the diffusion of ultra-shallow implanted B in α-Si using a SOI (silicon on insulator) substrate to suppress the SPER and hence to enlarge the range of annealing temperatures and times in the α phase.[10] They evidenced that the B diffusivity in α-Si is a transient phenomenon and it is enhanced at high

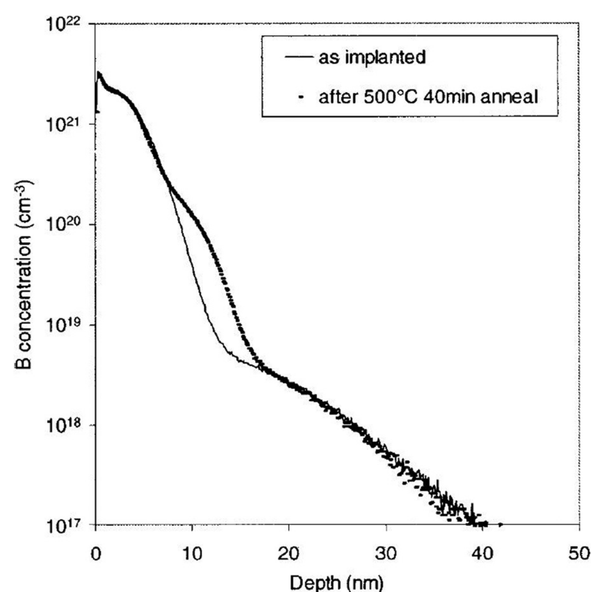

FIG. 2. Chemical profile of B as-implanted in α-Si (0.5 keV, 1×10^{15}/cm^2) and after annealing at 500 °C for 40 min. Reprinted from R. Duffy *et al.*, Appl. Phys. Lett. **84**, 4283 (2004). Copyright 2004 American Institute of Physics.

B concentrations, deviating from the Fick's laws and causing a concentration gradient which is not reduced after diffusion.

Actually, the B diffusion in α-Si can be appreciated only below the clustering threshold and in the region with the highest concentration gradient for the B profile. For ultra-low energy (0.5 keV) B implantation, this means above $\sim 5 \times 10^{18}$ B/cm^3, since below this concentration, the channeled portion of the profile hides the phenomenon (Fig. 2). To avoid this limit in the B diffusion investigation and to expand the annealing process window, we joined the SOI approach with the molecular beam epitaxy (MBE) growth of a structure with very high gradients in the B concentration profiles.[11] As sketched in the inset of Fig. 3, upon a SOI substrate, a 350 nm c-Si film was grown by MBE with two thin B doped regions at concentrations below ($\sim 7 \times 10^{19}$ B/cm^3) and above ($\sim 8 \times 10^{20}$ B/cm^3) the clustering threshold. The whole structure was amorphized by Si$^-$ implantation and thermally annealed in the 450-650 °C range for times shorter than the onset of the amorphous-crystalline transition. In such a way, the B diffusion phenomena were studied with high accuracy and over a larger dynamic range in the concentration values than in ultra-shallow B implantation experiments, also avoiding any dopant outdiffusion effect through the surface.

Fig. 3 confirms the clustering threshold at $\sim$1-2 $\times 10^{20}$ B/cm^3, evidenced by the kink in the high B box, and shows that the B diffusion in α-Si is much larger than in c-Si, for which the diffusion length after similar thermal budgets would be negligible.[40] In addition, Fig. 3 presents the unusual diffusion process, which does not lead to the expected long diffusion tails and to the reduction of the concentration gradients, but gives "box-like" shapes with wide shoulders and narrow tails. To explain this feature, a diffusion coefficient increasing with the B concentration (n_B) has been suggested.[10] Still, by looking at Fig. 3, for a fixed B concentration (e.g., $n_B = 1 \times 10^{19}$ B/cm^3), one observes a different broadening of the two B boxes, the larger for the higher B concentration box. Such an evidence excludes an univocal relation between D_B and n_B, suggesting that the migration process depends on the global amount of B in the surrounding, rather than the local concentration.

An effective B diffusivity (D_{eff}) can be hence estimated, for the two boxes, as the difference between the variance (σ^2) of the diffused B distribution with respect to the as-amorphized case ($\sigma^2{}_0$), divided by twice the annealing time (t): $D_{eff} = (\sigma^2 - \sigma^2{}_0)/2\,t$. These values are reported in Fig. 4 for the high (squares) and low (circles) B boxes, for all the annealing processes, together with the value at the same temperature of D_B in intrinsic c-Si multiplied by a factor of 10^5 (dotted horizontal line in Fig. 4); this points out the larger migration ability of B in α-Si with respect to c-Si. Moreover, D_{eff} is systematically higher in the high B box and an evident transient effect is observed in all the cases, with D_{eff} decreasing for both the boxes within a quite wide time scale. Such a transient phenomenon might be related to the relaxation of α-Si, assuming that the coordination defects mediate the B diffusion. Still, at all temperatures, the observed diffusivity transient is much longer (10 to 100 times) than the α-Si relaxation times reported in literature.[20]

Given these experimental features for B diffusion in α-Si, a simple formula for D_B as a function of the concentration cannot account for the complex aspects of the phenomenon. In summary, the B migration in α-Si: (i) has a transient character, which cannot be explained only with the well-known relaxation of α-Si; (ii) has a non-trivial concentration dependence, which determines a larger diffusivity, the greater the global amount of B in the surroundings is. In order to describe the B migration in α-Si, the interplay between B atoms and coordination defects has to be revealed and a precise modeling needs to be employed, as presented in Sec. II C.

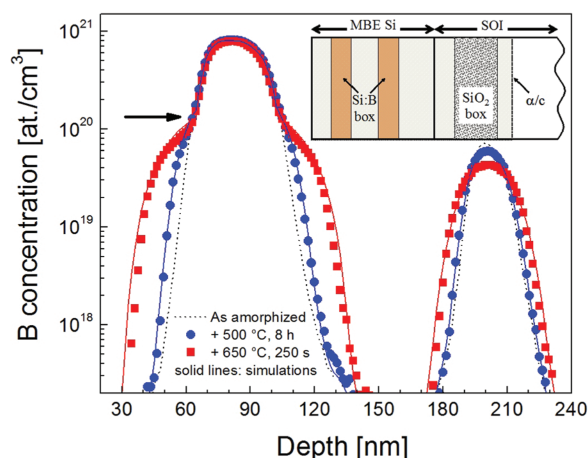

FIG. 3. Chemical profile of B in the as-amorphized sample (dotted line) and after annealing at 500 °C, 8 h (circles) or 650 °C, 250 s (squares), with the simulations following the best fit procedures (solid lines). Experimental drawing in the inset. Reprinted with permission from S. Mirabella *et al.*, Phys. Rev. Lett. **100**, 155901 (2008). Copyright (2008) The American Physical Society.

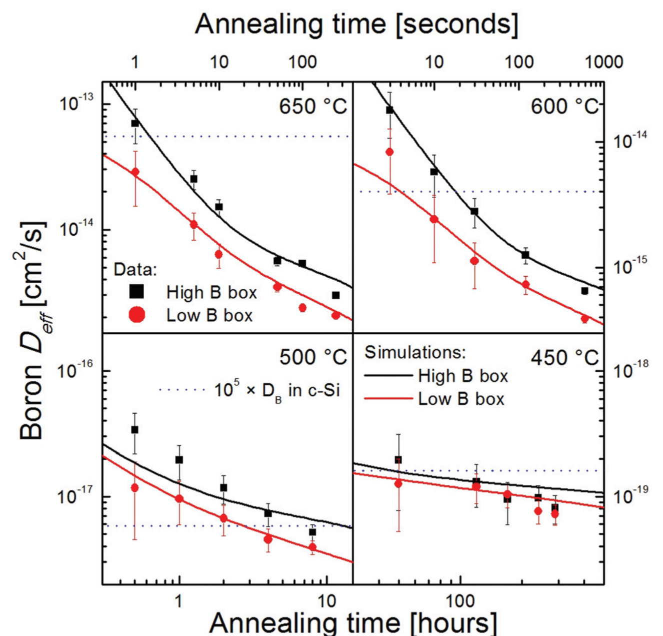

FIG. 4. Transient effect in the effective B diffusivity measured in the high (squares) and the low (circles) B boxes, with simulation curves (solid lines). Dotted lines represent the B diffusivity in c-Si multiplied by a 10^5 factor, for each annealing temperature.

C. Defect assisted B diffusion

As observed above, the unusual concentration dependence of D_B seems to be related to the overall amount of impurities, since larger B diffusivity was measured in the high B box, for a fixed B concentration. To find out if there is any effect of the high B concentration on the coordination defects density in α-Si, Cu decoration technique was employed since Cu atoms bind with unsaturated bonds as those present in *db* or *fb* defects.[41] In such a way, a Cu chemical profile is somewhat proportional to the defect density. We compared this Cu signal in an α-Si layer (350 nm thick) undoped or B enriched (8×10^{20}/cm^3), both in the unrelaxed and in the relaxed state (i.e., after annealing at 500 °C, 1 h). After Cu implantation (15 keV and 1×10^{16}/cm^2), we induced Cu diffusion and defect decoration by annealing the samples at 200 °C for 1 h (such an annealing does not have a significant effect on the relaxation status of α-Si[20]). Figure 5 presents the obtained Cu profiles, revealing that B enriched α-Si layers are 2-3 times richer in defects than undoped matrices, both in the unrelaxed and in the relaxed state. Such a significant effect of B in steadily increasing the defect density in α-Si can be joined with what observed by Muller *et al.*,[37] according to which in thermally relaxed α-Si impurities such as B are usually incorporated within 3-fold coordination sites. In fact, it is very reasonable that a B atom, 4-fold coordinated in c-Si, upon amorphization is accommodated into a 3-fold coordinated site, breaking one Si-B bond and generating an excess of *db* in the network. Actually, Muller *et al.* proposed that in hydrogenated α-Si these *db* excess is saturated by H,[38] still in non-hydrogenated α-Si, we can assume that such an excess in coordination defects can be distributed into the network, greatly affecting the diffusion of impurities.

In the following, such a *db* excess is exploited to model the collected data by assuming that B migration in α-Si occurs via an indirect mechanism. Boron jumps between adjacent 3-fold coordination sites through the temporary restoring of a metastable 4-fold coordinated B, by the capture and release of one *db*, as follows:

$$B_3 + db \leftrightarrow B_4. \tag{2.1}$$

The time evolution of the B profile has to be modeled in conjunction with the time evolution of the *db* population, whose density is transiently increased just after ion implantation or permanently enhanced by the presence of boron atoms themselves. The B migration in α-Si has been hence satisfactorily simulated (solid lines in Fig. 3) with the following rate equations:

$$\frac{\partial n_B}{\partial t} = \alpha \frac{\partial^2 (n_B \cdot n_d)}{\partial x^2}, \tag{2.2}$$

$$\frac{\partial n_d}{\partial t} = \alpha \frac{\partial^2}{\partial x^2}(n_B \cdot n_d) + D_d \frac{\partial^2 n_d}{\partial x^2} - 4\pi a (D_d + D_f) n_d \cdot n_f, \tag{2.3}$$

$$\frac{\partial n_f}{\partial t} = D_f \frac{\partial^2 n_f}{\partial x^2} - 4\pi a (D_d + D_f) n_d \cdot n_f, \tag{2.4}$$

where n and D are the concentration and diffusivity of the subscript species (B for Boron, d for *db*, f for *fb*), respectively. Equation (2.2) describes the time evolution of B concentration under the hypothesis that the mass flux of B is proportional (by the constant α) to the encounter probability of *db* and B. Then, Eq. (2.3) describes the time evolution of *db*, considering three terms: (i) the B-*db* coupled diffusion term, (ii) the Fick-like diffusion term, (iii) the annihilation term (supposed occurring through a *db*–*fb* meeting), whose capture radius (a) is assumed equal to the second nearest neighborhood distance (0.385 nm) in Si lattice. Time evolution of *fb* density (Eq. (2.4)) comprises only the last two terms. The concentration of B, *db*, and *fb* should be fixed at some starting conditions. The starting value of n_B (mobile B) is given by the chemical profile below a threshold density (n_c) caused by the B clustering (assumed to be instantaneous and time independent). The starting n_d and n_f profiles have a common homogeneous component n_0, representing the *db* and *fb* density after amorphization. Then, n_d has an additional contribute due to the B effect (as observed in Fig. 5) that is proportional (by a coefficient γ) to the starting, un-clustered B concentration. The free, temperature dependent parameters of the model are: n_c, α, and D_d (reasonably fixed equal to D_f), while n_0 and γ, being relative to the initial conditions of the α-Si matrix, are considered temperature independent and are simultaneously fitted for all the temperatures. All the free parameters have been fixed by satisfactorily fitting more than 20 profiles containing both the B boxes (see Fig. 3 as an example). n_0 resulted to be about 1.8 at. %, in agreement to literature data.[20,23,42] γ resulted to be 1.0 ± 0.5, confirming that one excess *db* is generated by one un-clustered B atom in amorphized Si. n_c was found to be temperature independent, with a value of about 2.2×10^{20} B/cm^3, again in full agreement with literature indications.[10] Finally, the Arrhenius plots for the fit results of the main physical parameters, α (circles, right vertical axis) and D_d (squares, left vertical axis), are shown in Fig. 6.

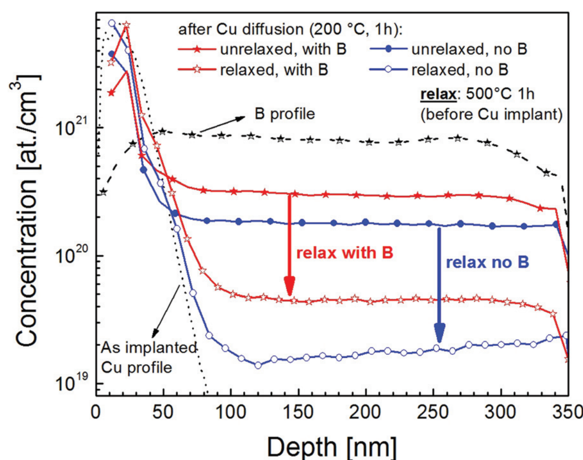

FIG. 5. Cu decoration technique for profiling the coordination defects in undoped (circles) or 8×10^{20} B/cm^3 enriched (stars) α-Si. Cu was implanted (dotted line, 15 keV, 1×10^{16}/cm^2) in unrelaxed (closed symbols) and relaxed (open symbols) samples, and Cu profiles have been measured after diffusion annealing at 200 °C, 1 h. Cu concentration in undoped Si is lower than in B enriched Si, regardless of the relax status.

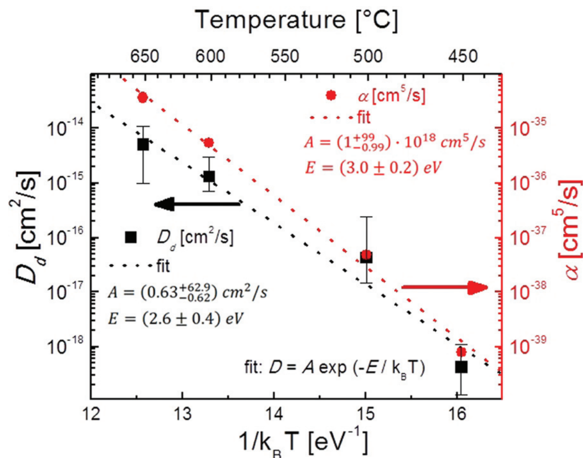

FIG. 6. Arrhenius plot for the diffusivities of dangling bond (D_d, left axis) and of B per unit of dangling bond density (α, right axis), with the relative fits (dotted lines) and equations. Reprinted with permission from S. Mirabella *et al.*, Phys. Rev. Lett. **100**, 155901 (2008). Copyright (2008) The American Physical Society.

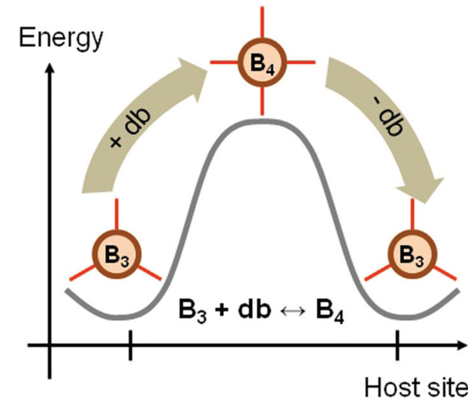

FIG. 7. Schematic representation of the atomistic mechanism of B diffusion in amorphous Si. An immobile, 3-fold coordinated, B atom jumps to an adjacent site through the exchange of a dangling bond (*db*) and the temporary restoring of a metastable, 4-fold coordinated configuration.

The proposed model is able to explain both the peculiar concentration dependence and the transient behavior of B diffusion in α-Si. The concentration dependent diffusion is simulated considering that the higher the B density, the more *db* are present, promoting a faster B diffusion. The excess of *db* is higher in the higher doped regions, accounting for the wider tail broadening in the high B box. On the other hand, the transient diffusion is related to two distinct causes for *db* density reduction. The first one is the *db*–*fb* annihilation (whose rate is in agreement with literature data[20]), which quickly reduces the B diffusivity in the early stages of annealing. The second cause is the progressive reduction of *db* density due to *db* diffusion itself. Both phenomena are regulated by D_d, but have quite different time scales. The non local diffusion effect is properly taken into account by the fact that *db* diffusion is faster than the B-*db* coupled diffusion, leading to a *db* profile larger than the B one. As a consequence, tail broadening of B profile largely depends on the local *db* density. As shown in Fig. 6, both *db* and B diffusivities span over six orders of magnitude and each one is well fitted by a single Arrhenius law. Both the diffusivities show quite similar activation energies, indicating that the B migration barrier is approximately fixed by the *db* diffusion barrier.

Figure 7 draws the microscopic mechanism proposed for B migration, through the interconversion between 3-fold (immobile) and 4-fold (saddle point) coordinated configurations, requiring the exchange of a *db* with the hosting matrix. The energy barrier to B diffusion (the height of the saddle in the figure) is fixed by the activation energy for *db* diffusion.

Recently, such a microscopic picture has been used by Martin-Bragado and Zographos from the Synopsys Inc. to generate a kinetic Monte Carlo (KMC) model for B diffusion in α-Si.[43] The above hypotheses have been employed within the KMC model which, once calibrated, was successfully applied to MBE grown B marker layers and also to ultra-shallow B implanted into preamorphized Si, confirming that the atomistic picture is able to simulate the B diffusion in α-Si under different conditions. According to the results reviewed here, B migration in α-Si is going to have a larger and larger role, especially for future technologies employing preamorphization steps and reduced thermal budgets.

III. B DIFFUSION IN c-Si: ATOMISTIC MECHANISM, ENERGETICS AND CLUSTERING

A. Milestones on the B diffusion mechanism

The investigation of B diffusion in c-Si represents an ideal case for impurity migration in a solid matrix, due to the exceptional high purity and accuracy in the material synthesis and analysis. There has been a great interest in this scientific topic, an almost forty-year investigated case with thousands of papers, also inspired by its application in the continuous scaling down of microelectronic devices. In the following, some of the most relevant findings will be reviewed, evidencing how new concepts for B diffusion have arisen and been developed over the time.

In 1975, Fair and coworkers proposed that the diffusion of B in Si is controlled by donor-type monovacancies, mainly basing this idea on the experimental evidence (Fig. 8) that the B diffusivity increases with B concentration under extrinsic doping conditions.[44] Such a result, obtained from ion-implanted B in Si in presence of an uniform doping background, shows a nice linear dependence of D_B versus the p/n_i ratio (n_i being the intrinsic electron concentration and p the hole density) over almost three orders of magnitude, regardless of the used dopant or the doping technique (implantation, pre-deposition, or doped-oxide source). Since the concentration of singly charged vacancy V^+ is proportional to the p-type dopant concentration, the $B_{S-} + V^+ \rightarrow B_m$ interaction could actually account for the extrinsic effect in the B diffusion (being B_S^- a substitutional B ion, and B_m a mobile B).

At the same time, a role for self-interstitials in the B diffusion was first pointed-out by Hu, showing the close relationship between two phenomena occurring during the thermal oxidation of Si: the formation of stacking faults and the enhanced diffusion of B.[45] Thus, B is assumed to diffuse through a dual mechanism, with a dominant interstitialcy

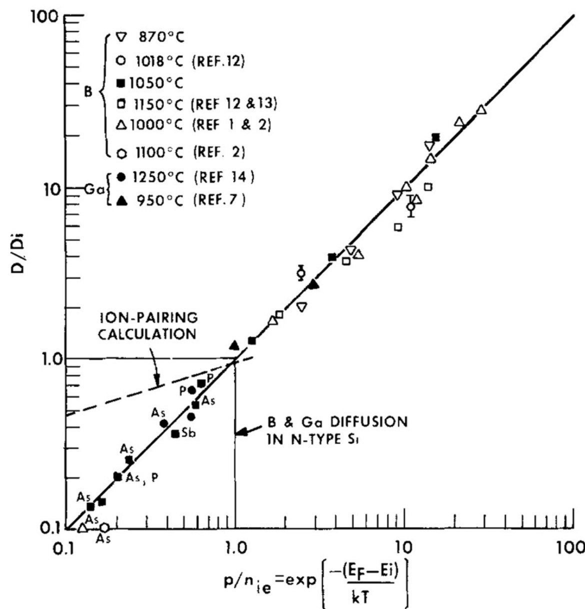

FIG. 8. Diffusivity of Boron and Gallium in silicon as a function of the normalized hole concentration. The linear trend over almost three orders of magnitude indicates that the mobile B*I* pair is in the neutral charge state. Reprinted with permission from R. B. Fair and P. N. Pappas, J. Electrochem. Soc. **122**, 1241 (1975). Copyright 1975 The Electrochemical Society.

component.[45] Following this assumption, the concept of fractional interstitialcy mechanism (f_I) was introduced as the fraction of diffusivity, which can be ascribed to an *I*-mediated mechanism.[46] Since 1982, numerous experimental determinations of the f_I fraction for B were given by several authors[40,46–51] through accurate selective modification of the native-point defects concentration (via surface oxidation for enhancing *I* density or nitridation for suppressing it) and measurement of the related B diffusivity. The very large value measured for f_I brought to the well-assessed conclusion that B diffusion in c-Si is exclusively mediated by self-interstitials, excluding any role for vacancies. Such a conclusion was also supported by the calculations of Nichols and coworkers,[52] which stated that the exchange mechanism should have a minor role for B diffusion.

The possible mechanisms for *I*-mediated B diffusion are the kick-out and the interstitialcy reactions, where the interaction between a substitutional B and a self-interstitial leads to a mobile species formed by an interstitial B or a B*I* couple, respectively,

$$B_S + I \rightarrow (B_i)_{mobile}(\text{kick} - \text{out}), \quad (3.1)$$

$$B_S + I \rightarrow (BI)_{mobile}(\text{interstitialcy}). \quad (3.2)$$

From an experimental point of view, it is hard to distinguish between them, since no difference are caused in the diffused profile. Still, some early theoretical investigations of the energetics of B diffusion revealed that the preferred migration pathway is the kick-out process, so that the diffusing species is the interstitial impurity atom.[52,53] More recently, advanced calculations gave a new vision of the B diffusion mechanism, showing that the intermediate mobile species is not the interstitial B but the B*I* pair.[2,3,54] Later on, using an atomistic kinetic Monte Carlo method joined with a continuum approach, Martin-Bragado *et al.* found that among all the charge states of mobile boron (either as interstitial boron or as B*I* pair), the positively charged one has the lowest formation energy, still the migrating species is found to be the neutral one, thus some interconversion between different charge states should occur for the diffusion process.[55]

Once more, the calculation of energetics and molecular dynamics simulations gave a valuable insight into the microscopic mechanism of B diffusion, especially for the possible charge states and the Fermi level effect, while the verification of these hypotheses require well prepared and accurate experiments.

Basing on the interstitial mediated process for B in Si, Nick Cowern and co-workers gave the first experimental evidence that impurity diffusion can proceed through an intermediate temporary species formed after the interaction with native-point defects. They investigated the migration of B in Si through chemical profiling of a narrow MBE-grown B profile and appropriate modeling based on the interstitial mediated process.[1,56] Within this model, substitutional (immobile) B can be converted (with a frequency rate, g) into a migrating species after a proper interaction with I. Hence, B diffusion occurs thanks to the formation of mobile B, and goes on up to its recombination into substitutional form. Thus, the B diffusivity is given by $D = g\lambda^2$, where λ is the mean projected path length for mobile B between its formation and recombination.

The main visible feature of this mechanism is that if λ is long enough and if the mean number of B diffusion events per each B atom is lower than or about one, the diffused profile of a starting delta doping strongly deviates from the expected Gaussian shape, revealing long exponential tails as the results of the long migration length. Such a deviation from the Fick's law is expected, since the flux of migrating species is not purely determined by the local gradient in the substitutional impurity concentration. Fig. 9 reveals the difference between B diffusion at 900 °C in inert ambient or at 625 °C in oxidizing ambient (which increases the *I* density), with a Gaussian shape or exponential tails, respectively. At the lower temperature, the number of diffusion events

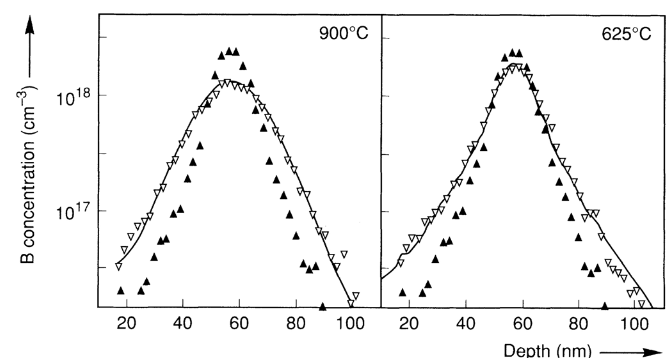

FIG. 9. Diffusion of a B delta (grown by molecular beam epitaxy) annealed at 900 °C for 5 min in N_2 ambient (left panel) or at 625 °C for 110 h in dry O_2 ambient (right panel). The different shapes of the diffused profiles were simulated (continuous lines) with the interstitial mediated diffusion model. Reprinted with permission from N. E. B. Cowern *et al.*, Phys. Rev. Lett. **67**, 212 (1991). Copyright (1991) The American Physical Society.

experienced by each B atom (gt, where t is the diffusion time) was calculated to be 0.4 and the migration length is 10 nm (causing the long tails), while at 900 °C, gt is larger than 3 and λ is lower than 5 nm. Definitively, the Gaussian limit is approached only if each B atom experiences more than one diffusion event and, thus, in these conditions, the Fick's law properly describes the B migration. In the case of low gt values, the microscopic mechanism of B diffusion through the intermediate species formation comes into sight and a proper simulation code based on the migration rate (g) is needed. In this way, the value of g and λ have been determined showing that an oxidizing ambient enhances only the formation rate of mobile B, while the migration length is unaffected. This fact evidences that the interstitial density enhancement due to oxidation helps the B migration rate, while the inverse reaction, independent of the interstitial density, decreases with temperature because of the energy barrier to the conversion of mobile B into substitutional B.[56]

Given the crucial role of *Is* in B diffusion, any variation of the density of these point-defects (PDs) can heavily affect the B migration. In fact, beyond the surface oxidation, a further and more efficient way to increase the *I* density is the ion implantation followed by thermal annealing, which produces an *Is* excess roughly equal to the implanted ion dose ("plus one model"[57–59]). The *Is* excess increases the B diffusivity, as shown since 1973 with an enhanced diffusion of B atoms implanted in Si.[60,61] Such a non-equilibrium phenomenon revealed a transitory feature, lasting for about 45 min at 800 °C and some seconds at 1000 °C,[62] deserving the name of transient enhanced diffusion (TED). The cause of this effect was discovered in mid nineties[63,64] and clearly attributed to the simultaneous thermal dissolution of *{311}* defects (extended rod-like *I* clusters displaced on {311} habit planes) formed as a consequence of the coalescence of the implant damage. The TED of boron has been very largely investigated, and many features were reported in excellent review papers as Refs. 4 and 65, so here no further details will be given about it. A further, non negligible effect of a large *I* supersaturation is the formation of B-*I* clusters (BICs), which trap diffusing B atoms and host its electrical activation. These aspects will be separately treated in the Sec. III D, while here the B diffusion without clustering will be reported.

B. Atomistic pathways of B diffusion

In order to discriminate between the different reaction paths and charge states involved in B diffusion in Si, we investigated the atomistic parameters (g and λ) of B diffusion in Si as a function of the hole concentration.[66] First, boron profiling with secondary ion mass spectrometry (SIMS) has been developed with high accuracy and sensitivity. The improvement of the technique consisted in cooling the samples at −70 °C, in order to suppress the long-range anomalous diffusion of B occurring at room temperature during the analysis and thus distorting the profiles,[67] and in flooding the samples with oxygen during the analysis, for enhancing the measurement sensitivity by a factor of 20.[68] The use of the above measurement protocol and a diffusion simulation code based on Cowern's rate equations[1,56] allowed us to determine, with utmost accuracy and sensitivity, the microscopic diffusion parameters of a sharp ^{11}B spike embedded in different ^{10}B, P, and As backgrounds.

The different migration features of B in c-Si when moving the Fermi level position can be appreciated in Fig. 10, where we compare two diffusion processes performed at 700 °C on the same ^{11}B delta but embedded in a n-type or p-type background doping. Different annealing times were used to achieve a comparable overall diffusion (1 or 7.5 h for the p or n-type case, respectively), evidencing a much higher diffusivity in the case of p-type doping background, as expected, and a substantial divergence in the shapes of the two diffused profiles. If we look at the top portion of the diffused profiles, the p-type case presents the highest shape, while as far as the tail parts are concerned, the same sample shows unexpectedly the larger profile (evidencing a larger mean diffusion length, λ, as extracted by the best-fit procedure). Typically, the diffusion broadening proceeds via a concomitant lowering of the top profile and widening of the tails. Still, here the experimental data show that the two diffusion processes occur with quite different migration lengths, the longer in the p-type doping case. The lines are the best fits to the diffused data obtained by numerically "'diffusing'" the profile according to the equations of Refs. 1 and 56. To get more insight on the microscopic mechanism of B atomic transport, we repeated the same analysis with isothermal annealing after moving the Fermi level position by doping and thus varying the free carrier concentration by almost four orders of magnitude (going from heavily p-type to heavily n-type doping background).

The diffusion parameters D, g, and λ (extracted by the best-fit procedure) have been reported synoptically in Fig. 11, as a function of the hole concentration normalized to the intrinsic carrier concentration (p/n_i, n_i equal to 0.92 $\times 10^{18}$ /cm^3 at 700 °C,[40] p is calculated starting from the background doping concentration according to Boltzmann statistics and considering a full ionization of the dopants).

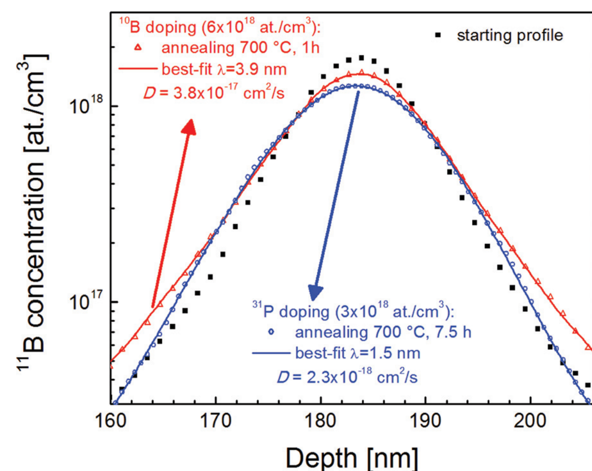

FIG. 10. Chemical profile (symbols) of ^{11}B spike before (squares) and after diffusion annealing at 700 °C for the samples with different doping backgrounds (triangles for ^{10}B doping or circles for ^{31}P doping). The continuous lines are the best fits to the data.

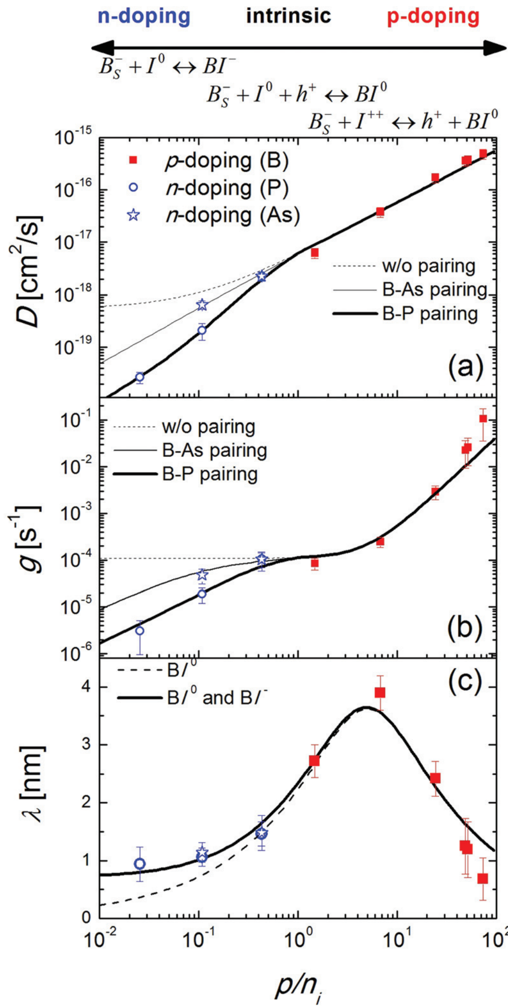

FIG. 11. Diffusivity (a), migration rate (b), and mean diffusion length (c) as a function of p/n_i (hole concentration normalized to the intrinsic carrier concentration at 700 °C, equal to 0.92 × 10^{18}/cm^3 (Ref. 40)). Symbols are referred to experimental data (squares to B doping, circles to P doping and stars to As doping) while lines are simulation based on the models in Ref. 14 considering or not the B pairing with As or P (a) and (b), and the B mobile species as the BI^0 complex with or without the BI^-complex (c). Above the graph, the varying doping condition together with the main reaction leading to the diffusion have been indicated.

The diffusivity [Fig. 11(a)] in the case of intrinsic or p-type doping shows a linear increase with the hole concentration [well fitted by the relation: $D = D_0(p/n_i)$]. Such a trend is univocally connected to the charge state of the mobile BI complex, since it says that the whole diffusion process proceeds by the net exchange of a single positive charge (whose density increases linearly with p/n_i). In the case of n-type doping, the diffusivity is strongly suppressed as a result of the Coulomb attraction between the B and n-type dopants leading to a pairing effect.[69] Such pairing is stronger in the case of P doping than for As doping, reducing the diffusivity to larger extent in the former case.

The g and λ trends (panels (b) and (c) in Fig. 11, respectively) explain into much deeper details the microscopic migration paths involved at different Fermi level positions. In the case of intrinsic or p-type doping, the g trend as a function of the hole density shows a constant component together with a quadratic one, as follows:

$$g = g_{I0} + g_{I++}(p/n_i)^2. \tag{3.3}$$

This can be thought as if the B-I interaction, leading to B diffusion, is driven by neutral I^0 or by doubly positive I^{++}, since the density of I^0 and I^{++} have a constant and a quadratic trend with p/n_i, respectively.[40] As a consequence, in the intrinsic case, a BI complex in negatively charged state is produced, while in p-type doping, a single positively charged BI pair is given, as follows:

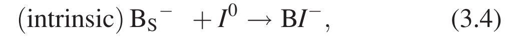

$$(\text{intrinsic})\, B_S^- \; + I^0 \rightarrow BI^-, \tag{3.4}$$

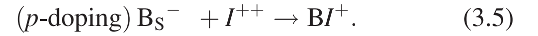

$$(p\text{-doping})\, B_S^- \; + I^{++} \rightarrow BI^+. \tag{3.5}$$

Nevertheless, the diffusing species is BI^0, thus both the above charged BI complexes should undergo an interconversion by changing their charge state through a free carrier exchange.

The λ trend clarifies this point, since it represents the mean free path of the diffusing species. The bell shape traced by λ as a function of p/n_i is the consequence of the charge exchange needed to transform BI^- and BI^+ species into the mobile BI^0 form. When p/n_i is lower than 4, BI^- is produced in essence, and it has to get a hole to move, so BI mean free path increases by increasing the hole availability (i.e., by increasing p/n_i). On the contrary, when p/n_i is larger than 4, BI^+ is produced, and it has to lose a hole to move. This is less probable to occur the higher is p, thus reducing its free mean path (λ).

As far as the pairing is concerned, the λ trend evidences no difference between P or As doping, while g is reduced in different ways for the case of P or As n-type doping. The trend of g in the case of n-type doping reveals that the formation of the mobile B species is less favored in the case of P doping with respect to the As doping. Data modeling allowed to estimate the Coulomb pairing energies to be 0.7 or 0.5 eV for the B-P or the B-As pair.[14] This pairing lowers the energy of substitutional B and then increases the energy barrier to the formation of the mobile B species. The ion pairing is not expected to influence the migration length of mobile B (as the B-P or the B-As mean distance is well larger than the measured λ values). This fact is confirmed by data, showing no difference in λ trend between P and As doping. On the other hand, the migration length should go to zero when p/n_i is reduced, since no holes are available to induce the BI^-→ BI^0 reaction. This is not the case (Fig. 11, panel (c)). This can be explained considering a small contribution to the B diffusion has to come from the BI^- complex, which appears to be the only mobile species under n-type doping.

The full reactions leading to the B diffusion in the intrinsic and in the p-type or n-type doping are reported in the top portion of Figure 11. It has been consolidated that the main diffusing species is the BI^0 complex, while a small contribution of the BI^- complex is visible only under n-type doping where BI^0 production is strongly depleted. Preferential interactions of B_S^- with I^0 or with I^{++} have been evidenced in intrinsic conditions or high hole densities, respectively, followed by charge exchange towards the formation of the diffusing BI^0 complex, while for n-type doping B_S^- and I^0

form the BI^- complex responsible for the diffusion. In the last case, the formation of the mobile B species is depressed by the pairing of B with n-dopants, which increases the energy barrier to the reaction with the self-interstitial.

The above scenario detailing the diffusion paths of B when moving the Fermi-level position was largely confirmed by an independent experimental approach performed by Bracht and co-workers in 2007.[70] Through the experimental investigation and simulation of simultaneous diffusion of dopants and self-atoms in the p-type or n-type doping conditions, it was demonstrated that diffused B profiles are mainly sensitive to model parameters such as the diffusivities of I^0, I^+, I^{++}, and Bi^0, indicating that the neutral and positively charged Is contribute to B diffusion and that some charge exchanges occur since the migrating species is assumed to be the neutral B_i^0. They also showed that under high B doping levels, B diffusion is mainly mediated by I^{++}, confirming our picture for high hole density. Moreover, from data in Ref. 70, it can be calculated that the I^+ contribution to g is always less than 10% at all experimental temperatures in intrinsic and p-type doping conditions, confirming that the dominant channels are through I^0 and I^{++} interactions. It should be noted that, by studying the simultaneous B and self-diffusion, Bracht and co-workers also found some preliminary indications that B diffusion could occur through a kick-out reaction rather than an interstitialcy mechanism, which would have caused a non-observed contribution of BI pairs to the self-diffusion. However, further calculations of the correlation factors of self-diffusion via the BI pairs are required to clarify this point.[70]

The two independent experimental investigations of the B migration have been compared by Windl in 2008, looking for a common description of the diffusion phenomenon. After deriving the activation energies for B diffusivity, generation rate and mean free path from the experimental data and mapping them versus the Fermi-level representation (commonly used to display *ab-initio* results), Windl showed that the experimental results are consistent with each other and with their theoretical values.[71] A strong role of I^0 and I^{++} in B diffusion was confirmed, while a low theoretical value for the activation energy of I^+ has been postulated. One could assume that at temperatures at which diffusion really occurs, both energetic and entropic factors affect the phenomena and thus a very low entropic prefactor for I^+ could justify the experimental evidence that the B diffusion is essentially dominated by I^0 and I^{++}.[14]

Thus, once fixed the diffusion pathways through the interaction of substitutional B with neutral or doubly positively charged self-interstitials, a quantitative investigation of the atomistic parameters at different temperatures is needed to measure all the energy barriers to B diffusion.

C. Energetics of B diffusion

The same experimental approach of a sharp ^{11}B spike embedded in different doping backgrounds was used to determine the diffusion parameters (D, g, and λ) in the temperature range between 610 and 810 °C.[14] Figure 12 in the upper panel shows the diffusivity data divided by the p/n_i

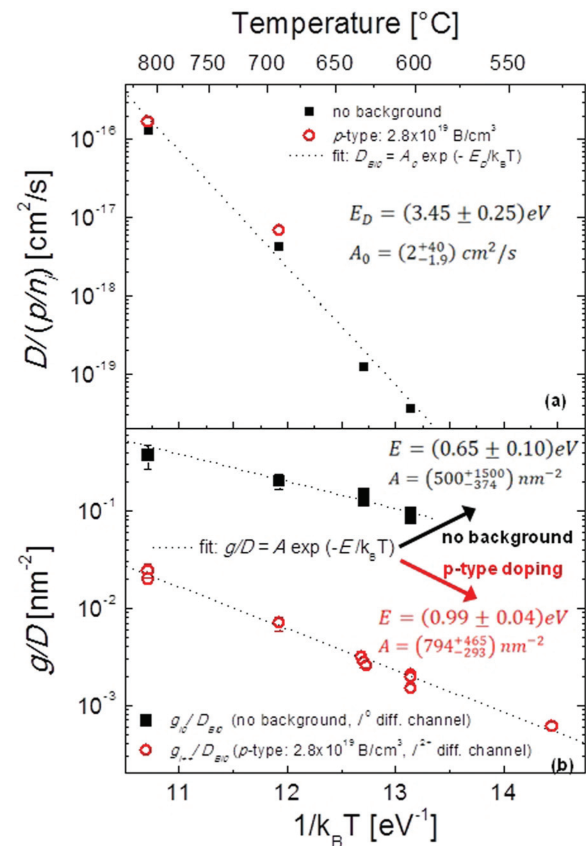

FIG. 12. Arrhenius plot of (a) diffusivity divided by p/n_i (hole concentration normalized to the intrinsic carrier concentration) and of (b) migration frequency divided by the diffusivity, as extracted from diffusion of a ^{11}B spike in intrinsic (closed squares) or p-type doped (open circles) conditions. Upper panel shows the energy barrier to the diffusion of the mobile BI^0 species. Lower panel represents the energy barriers to the formation of the BI^- or BI^+ complex (in the two diffusion channels), with respect to the energy level of the diffusing BI^0 complex.

values for a sharp ^{11}B spike under intrinsic conditions (without a doping background, closed squares) and with a constant background doping (2.8×10^{19} B/cm^3, open circles). Basing on the relation $D = D_0(p/n_i)$, the reported data represent the temperature trend of the diffusion component through the neutral BI^0 species, regardless if the BI^0 complex comes from intrinsic or p-type doping conditions. As can be noted, all the data fall to a good approximation on a single Arrhenius plot with an activation energy and a prefactor of 3.45 $\pm$ 0.25 eV and $(2^{+40}_{-1.9})$ cm^2/s, respectively. These results are in good agreement with the data found in literature for B diffusion under intrinsic conditions also at higher temperatures.[70] On this basis, it can be very reasonably stated that a single dominating diffusing process acts from 610 to 1100 °C demonstrating that the BI^0 diffusing species dominates the diffusion in a very large range of temperatures for intrinsic materials. The activation energy of 3.45 eV represents the energy barrier to the overall diffusion process under intrinsic conditions, which is essentially the energy cost paid by a B atom to change its status from the substitutional position (B_S^-) into the migrating species (BI^0). Actually, we demonstrated that this occurs through different pathways involving I^0 and I^{++}, so a further analysis is needed to

determine the energetics for the formation of the BI^-or the BI^+ complex, according to the reactions in Eqs. (3.4) and (3.5).

Figure 12 (lower panel) shows the temperature trends for the formation rates of the BI^- complex ($g_{I0}/D_{BI0,}$ closed squares) or the BI^+ complex ($g_{I++}/D_{BI0,}$ open circles) divided by the BI^0 diffusivity. These two quantities are related to the measured values of lambda in intrinsic and *p*-type doping conditions, as detailed in Ref. 14, and represent the energy barriers to the formation of the BI^- or BI^+ complex, with respect to the energy level of the diffusing BI^0 complex. Good Arrhenius trends are obtained for both the two cases and fitted with activation energies of (0.65 ± 0.10) eV or (0.99 ± 0.04) eV for the case of intrinsic or *p*-type conditions, respectively. This points out that the formation of the BI^-or the BI^+ complexes, needed to get the BI^0 mobile species, requires an extra energy with respect to the formation of the BI^0 mobile species, introducing a higher saddle point in the conversion process from the substitutional to the mobile B species, as it will be clarified in the following.

To get an overall vision of the B diffusion energetics, in Fig. 13 an energy scheme is reported. The basic diffusion process occurs with an energy cost (3.45 eV) that is the difference between the energy of the saddle point of diffusion of the BI^0 species and the energy of the substitutional B atom. Such an activation energy is deduced by considering the temperature dependence of the diffusion coefficient. Two possible diffusion species are BI^0 or BI^- pairs, the last one (not shown) being appreciable only under *n*-type conditions and responsible for less than 10% of diffusion in intrinsic condition.

When the temperature dependence of the formation rate is considered, a more detailed view appears, evidencing the two diffusion channels through the interaction with I^0 and I^{++} (as noted in Fig. 12) and their relative energy barriers. In intrinsic conditions, the I^0 path is much more convenient but, by moving toward *p*-doping conditions, I^{++} formation becomes favored as its energy cost reduces. The energy barriers to the formation of BI^- and BI^+ complexes starting from the substitutional B atom are 4.1 and 4.4 eV, respectively, as it can be derived from the 3.45 eV barrier plus the activation energies derived from Fig. 12. Finally, the introduction of *n*-type dopants lowers the starting energy level of substitutional B through the formation of pairs, which force a fraction of B atoms to have a much higher-energy cost for diffusion.

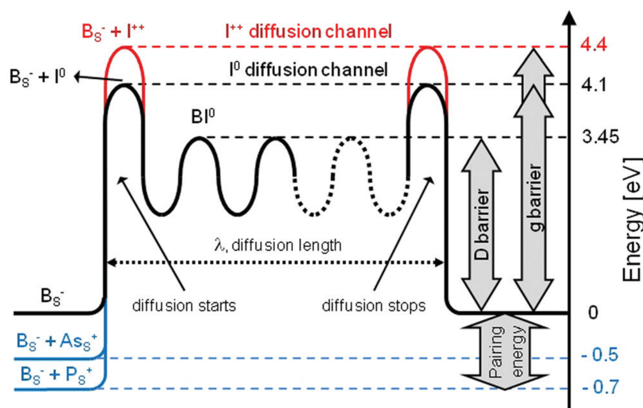

FIG. 13. Energetics of B diffusion process in crystalline Si. Substitutional B (B_S^-) can give mobile BI pair by interaction with I^0 or I^{++} with energy barriers of 4.1 and 4.4 eV, respectively. The BI species moves through negative BI^- (only in *n*-type conditions, not shown here) or neutral BI^0 saddle points. This last is the main mechanism with a 3.45 eV total activation energy. The pairing of substitutional B with As or P *n*-dopant is also indicated, causing a strong increase in the diffusion energy cost.

By summarizing the reported model for B diffusion, several physical processes are involved to quantitatively describe the atomistic mechanism of B diffusion in crystalline silicon: (i) the migration of B atoms starts after interaction of substitutional B with I^0 or I^{++}, leading to BI^- or BI^+ complexes; (ii) in intrinsic and *p*-type doping regime, the diffusing complex is a neutral BI^0 pair, involving a charge exchange mechanism; (iii) an alternative pathway for diffusion is constituted by a negatively charged BI^- complex that becomes significant only in the *n*-type doping regime; (iv) BI diffusion and Coulomb pairing effects of B with *n*-type dopants are disentangled and quantified. The presented model well accounts for the B diffusion process in absence of B trapping or precipitation. Actually, for a more comprehensive picture of the B diffusion process, further phenomena should be considered, among which the temporary immobilization of B atoms because of non-equilibrium precipitation into BIC, as treated in Sec. III D.

D. B-*I* clusters formation and dissolution

The evidence of B precipitation well below the equilibrium solid solubility in crystalline Si was given almost 40 years ago together with the early TED studies of B implanted in Si.[60–62,72] In the following, a concise selection of the numerous papers dedicated to this phenomenon will be presented, with the aim to elucidate the main issues which could affect the B diffusion.

Thermal annealing after B implantation (see Fig. 14) typically leads to a peak portion of the B profile, which is electrically inactive and immobile, and a lower part of the profile undergoing TED, with a concentration threshold about one order of magnitude below the B solid solubility.[72,73] Quite soon, it was proposed that the process responsible for the non equilibrium B precipitation through boron-interstitial clusters (BICs) formation was the same responsible for the TED effect, i.e., the *I* supersaturation.[73] Further confirmation of this came with the evidence that B clustering effectively contributes to lower the *I* supersaturation following ion implantation.[74] In addition, a proper substitutional B concentration was demonstrated to suppress the typical *{311}* defects, by a competitive BIC formation.[75]

The phenomenon of B-*I* clustering has a clear negative drawback as far as the dopant activation is concerned, but in addition, it has a weighty effect on the B diffusion process and on its simulation. In fact, B-*I* clustering affects the migration events not only because diffusing B atoms are trapped and later on de-trapped once BICs dissolve but also for the reason that the Si self-interstitial density is modified during BIC formation and dissolution, by *Is* hold and release processes from BICs. It was widely demonstrated that BICs

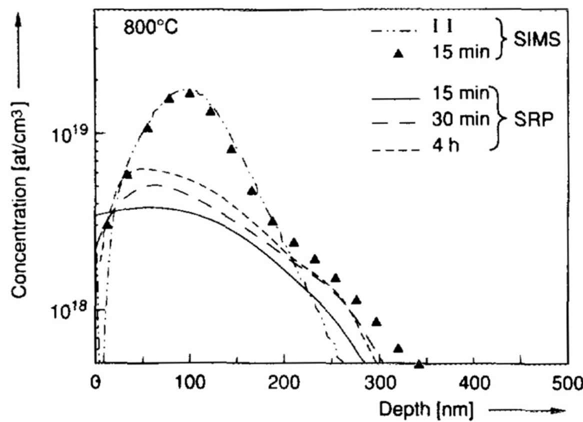

FIG. 14. Chemical (SIMS) and electrical (spreading resistance profiling, SRP) profiles of 25 keV, 2 × 10^{14} B/cm^2 implanted in crystalline Si and annealed at 800 °C for different times. The B profile is composed of an immobile, non-active part, and a diffusing part, with a concentration threshold at ~3 × 10^{18} B/cm^3. Reprinted from N. E. B. Cowern *et al.*, J. Appl. Phys. **66**, 6191 (1990). Copyright 1990 American Institute of Physics.

behave as a sink for *Is*, at the early annealing times, and as a moderate *I* source for longer times.[76–78] In this sense, the knowledge of the BICs features is essential to develop a complete simulation model of the B diffusion in Si.

Experimental investigations performed on MBE grown B multideltas (Fig. 15), implanted with Si ions, allowed to develop an atomistic simulation for B-*I* clustering and diffusion, disentangling the B doping from the implantation damage.[79,80] In the upper panel of Fig. 15, the chemical profiles of B delta doped layers are plotted before and after implantation and annealing, evidencing both the diffusion and the clustering caused by implantation. In the lower panel, the

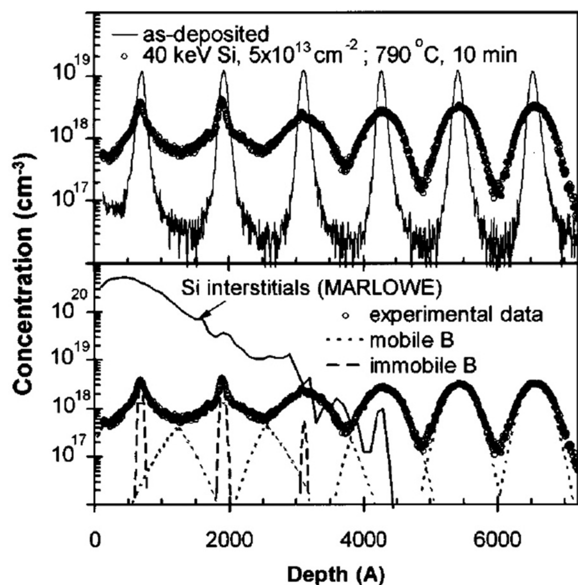

FIG. 15. Chemical profiles of a B multidelta structure grown by MBE and implanted with Si ions in the shallower region. (Upper panel) Thermal annealing at 790 °C induces the B TED in all the spikes, while the BIC formation causing the immobile peaks occurs only in the shallower region. Lower panel reports the simulation of the *Is* distribution after implantation and the de-convolution of the B profiles in mobile and immobile fractions. Reprinted from L. Pelaz *et al.*, Appl. Phys. Lett. **70**, 2285 (1997). Copyright 1997 American Institute of Physics.

simulations of the Si interstitials distribution and the mobile and immobile fractions of B profiles are reported. Basing on these results, it was argued that BICs: (i) form only in the region of high B concentration and high *I* supersaturation during implantation (as calculated from the MARLOWE code[79]), (ii) nucleate starting from an immobile precursor (BI_2) during implantation or at the very early stages of annealing, (iii) are of small size, with less than six atoms (so well below the transmission electron microscopy (TEM) detection limit), (iv) their thermal evolution proceeds via the emission of self-interstitials first and then B interstitials, up to the cluster dissolution.[80]

Several studies approached the phenomenon of B-*I* clustering in crystalline Si from a theoretical point of view, calculating the formation energy and structure of each plausible B-*I* cluster, the energetically favored B:Si stoichiometry, the possible pathways for BIC growth and dissolution and the interactions with *I*-type defects.[81–89] Most calculations provide such properties for small sized BICs (typically less than 10 atoms) and for a fixed structure or composition, while it cannot be excluded that an ensemble of different BICs size occurs in facts. Here, a major focus will be given on the experimental results on BIC sizes and dissolution barriers, which can be implemented for a viable simulation of the B diffusion process.

Given the very small size of BICs, TEM studies were lacking for a long time up to a few years ago, when first studies observed BICs as large as a few nanometers.[90,91] Weak-beam-dark-field (WBDF) analyses performed on high-dose, 0.5 keV B implanted crystalline Si, after a low-temperature annealing, evidenced the formation of large BICs (with hundreds of atoms) within the damage region.[90] Later on, large BICs have been observed also out of the implant damage region, by employing an MBE grown sample (containing a buried, highly doped B profile) subjected to shallow Si implantation (Fig. 16).[91] In this last case, the immobile B peak deduced from chemical profiling was found to overlap with the band of BICs observed by TEM (two dimensional

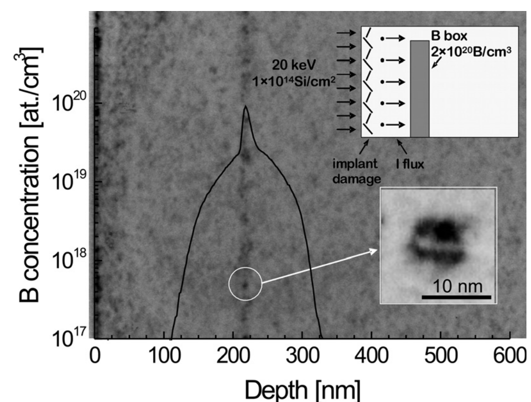

FIG. 16. Superimposition of BICs features observed by TEM (cross-sectional view) and chemical profiling (SIMS), taken from the same MBE sample (with an embedded B box) implanted with Si ions and annealed at 815 °C, 5 min. Small dark spots, with typical contrast of dislocation loops (as shown in the inset), are observed at the depth of 220 nm where the immobile part of the chemical profile is recorded. A schematic of the experiment is also shown. Reprinted from S. Boninelli, Appl. Phys. Lett. **91**, 031905 (2007). Copyright 2007 American Institute of Physics.

defects, with typical contrast of dislocation loops). The thermal dissolution of BICs was also followed by TEM imaging.[91]

Actually, the experimental determination of the dissolution kinetics at different annealing temperatures helps to understand the energetics of these clusters and to verify the theoreticians' calculations. Indeed, a quantitative analysis of BICs dissolution can be made by using chemical profiling (and the "diffusion criterion," i.e., clustered B is immobile) and/or electrical measurement (assuming that clustered B is electrically inactive). By quantitative high-resolution scanning capacitance microscopy, BICs were found to dissolve faster as the region where B clustering occurs is more confined.[92] BICs formation was induced by B implantation through submicron windows, and the total electrical activation is gained first in the narrowest window (0.38 μm), with times shorter by nearly a factor of 4 compared to the widest one (3.2 μm). Actually, the electrical measurements for quantifying the BIC dissolution can be affected by scattering effects by B clusters on the mobility of charge carriers, which alters the determination of the active B amount.[6,93–96] To properly measure the BIC dissolution energetics, we used the diffusion criterion together with a proper rate equation model able to fit the chemical profiles, to simulate the B diffusion and to extract the clustered B amount produced by a controlled *I* supersaturation into MBE grown Si samples containing various B doped regions.[97] It was clearly shown that B clusters dissolve following two distinct paths with different energy barriers (3.6 or 4.8 eV) and rates, the slowest one (with the 4.8 eV barrier) being present only for B concentration above the solid solubility.[98] Comparison with TEM studies suggested that the observed large BICs follow such a slow dissolution path,[91] while the faster path can be connected to mobile B direct emission from small clusters, not visible by TEM. Thus, BICs can be present in small sizes (below the nanometer scale and quickly dissolving), or in large sizes (observed by TEM and much more strongly bonded).

Basing on these evidences, very recently, Aboy *et al.* developed a comprehensive model for BIC formation and evolution in crystalline Si, including B_nI_m complexes quite larger than those included in previous atomistic simulations. BIC evolution is modeled as drawn in Fig. 17, considering exchange of B (oblique red lines) or Si (vertical blue lines) interstitials with the hosting lattice to change cluster configuration, and taking the formation energy of each B:Si cluster (referred to the perfect lattice) through comparison with theoretical calculations and fitting models to different sets of experimental data in literature.[96] In Fig. 17, four main regions have been defined, one region (SB, small BICs) for clusters with less than 4 B atoms, and three regions for large BICs (LBLI-large BICs low interstitial, LBB-large BICs barrier, and LBHI-large BICs high interstitial) with a larger number of B atoms. SB region includes small BICs ($n < 4$) that reproduce experimental data at low and medium B concentration; LBLI region considers very stable large BICs ($n > 4$, $m \ll n$) that form from SB region and only in the presence of high B concentration and low flux of *Is*; LBHI region with less stable large BICs ($n > 4$ and large amount of *Is*) coming from SB region if high B concentration and high flux of *Is* subsist; finally, LBB region represents quite unstable large BICs ($n > 4$ and intermediate amount of *Is*) that act as a barrier among less stable and very stable large BICs. Even if the largest BICs precipitate that can be included in such calculations contain less than 20 atoms, two different dissolution pathways have been found, a faster one for *I* rich BIC and a slower one for low *I* content, and the model has been successfully applied to BIC evolution in both B implanted and MBE grown Si samples.[96]

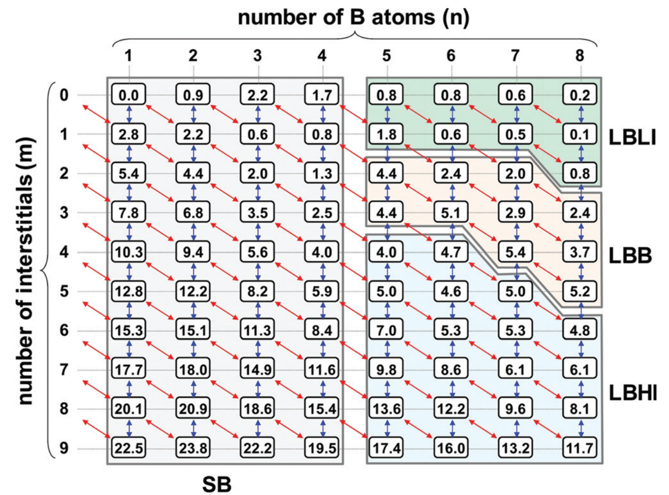

FIG. 17. Schematic map of B-*I* clusters energetics (referred to the perfect lattice) as a function of the composition (as B_nI_m clusters). BIC evolution towards different configuration occurs through B (oblique red lines) or Si (vertical blue lines) interstitials exchange with the hosting lattice. Four main regions have been defined: SB for clusters with less than 4 B atoms, LBLI (large BICs low interstitial), LBB (large BICs barrier), and LBHI (large BICs high interstitial) with a larger number of B atoms. Reprinted from M. Aboy *et al.*, J. Appl. Phys. **110**, 073524 (2011). Copyright 2011 American Institute of Physics.

Once clarified the main features of BICs formed in crystalline Si, some considerations should be done on B clusters occurring in amorphous Si and then transferred in crystalline Si. In fact, to avoid the overlapping of implant damage and dopant atoms, B is typically implanted in pre-amorphized Si followed by thermal induced SPER. Nevertheless, B clustering already occurs in pre-amorphized Si (cfr. Sec. II), even if to a lower extent than in crystalline Si, and then these clusters are transferred to the crystalline structure during the SPER.[6,12,13] Such B clusters, even if formed in preamorphized Si, can evolve towards BICs as large as 8 nm if a high B concentration is present and subjected to a proper *I* supersaturation, as shown by B chemical mapping and energy-filtered TEM investigations.[96]

In summary, the non equilibrium clustering of B induced by a supersaturation of *Is* gives out B:Si complexes, named BICs, whose size and thermal stability depend on the starting conditions. In any case, BICs have significant effects on the migration properties of B atoms by modifying both the concentration of mobile B atoms and the density of *Is*, thus B-*I* clusters should be taken into serious consideration when a complete modeling of B diffusion process is regarded.

IV. B DIFFUSION IN c-Ge: THE ROLE OF SELF-INTERSTITIALS

A. B doping in Ge

While B is by far the most used *p*-type dopant in Si, this is not true in Ge where the maximum solid solubility ($5 \times 10^{20}/cm^3$) among *p*-type dopants is reached by Ga.[16,99,100] Nonetheless, Satta and co-workers in 2005 showed that, if B is implanted in pre-amorphized Ge, a maximum activation level of $2.4 \times 10^{20}/cm^3$ is reached after solid-phase epitaxial regrowth at 400 °C.[101] Further investigations on B implanted in PAI-Ge, based on different analytic techniques, demonstrated that higher activation levels of B can be reached,[102] up to the maximum of $5.7 \times 10^{20}/cm^3$ after SPE at 360 °C.[19] These results support that B is a very good choice for *p*-type doping in Ge, also because its diffusivity is by far the lowest one among all the dopants in Ge.[18]

As far as B diffusion in Ge is concerned, the picture is not as much detailed as in silicon, neither there is a consolidated consensus on the microscopic mechanism leading to B motion. In amorphous germanium, no B diffusion was observed after the regrowth of a PAI Ge layer,[101] confirming the trend observed by Edelman and co-workers in amorphous SiGe alloys where the diffusivity decreases with increasing the Ge concentration.[103] Crystalline lattices of Si and Ge are very similar from the crystallographic and electronic points of view, but they are quite different as far as the dopant behavior is concerned. In c-Si dopants of the III and V groups diffuse by a PD mediated mechanism that can involve both vacancies (*V*s) and self-interstitials (*I*s), prevailing the former or the latter mechanism depending on the considered dopant. In contrast, in c-Ge, almost all dopants seem to diffuse by a *V*-mediated mechanism. This is attributed to the determination that *V*s in c-Ge play a dominant role with respect to *I*s, since *V*s are characterized by a formation energy ~1 eV lower than that of *Is*.[100] Still, the B migration in c-Ge represents a special case since its diffusion process seems to be different.

The investigation of B diffusion in c-Ge is hampered by a very small diffusivity. Fig. 18 shows that the diffusion of B implanted in Ge at 20 keV can be hardly appreciated even after annealing at 850 °C for 24 h.[17] Considering the Ge melting point at 937 °C, this datum evidences the very low B diffusivity in Ge. Bracht and co-workers, comparing D_B in Ge and in Si at homologous temperatures T/T_m (T_m is the melting point), showed that B diffusivity in Ge is 4-5 decades smaller than in Si.[18] B diffusivity in Ge measured under controlled conditions in the 800-900 °C range shows an activation energy of 4.65 eV, with a diffusion coefficient two orders of magnitude smaller than the smallest earlier estimate.[104] Based on its very low diffusivity and on the high activation energy, B diffusion through a *V*-mediated mechanism appears highly improbable. Actually, the activation energy for B diffusion in Ge is ~1.5 eV larger than that for self-diffusion and much larger than those of other common dopants diffusing via a *V*-mediated mechanism. An interstitial-mediated process was thus believed more conceivable.[104] In addition, the lack of stability of the B-*V* pair was also confirmed by some theoretical calculations.[105,106]

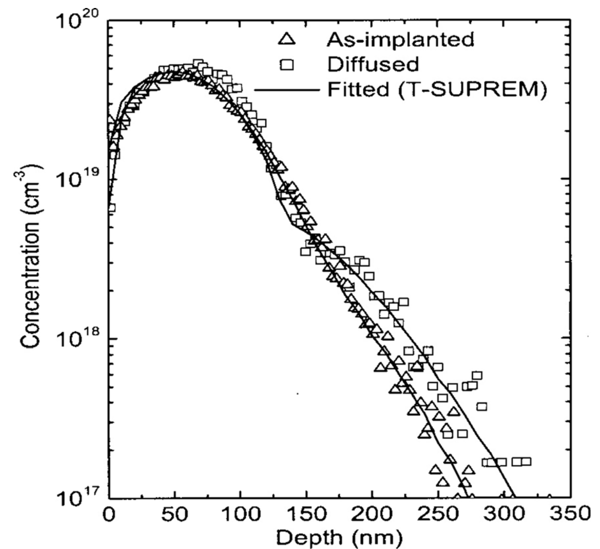

FIG. 18. Chemical profiles of B as-implanted in Ge (20 keV and $6\times10^{14}/cm^2$) and after annealing at 850 °C for 24 h, with fitting lines. Reprinted from S. Uppal *et al.*, J. Appl. Phys. **90**, 4293 (2001). Copyright 2001 American Institute of Physics.

Thus, for any experimental investigation of the B diffusion mechanism, non-standard conditions such as very long annealing times or annealing temperatures just below the melting point are required.

From a theoretical point of view, some works shed light on the possible migration mechanism in Ge, also comparing it with the well-assessed picture in the Si lattice. Via first principles calculations De Lugas and Fiorentini estimated the energetics and migration paths of boron in Ge, considering an *I*-mediated mechanism, specifically the g-λ mechanism previously associated with B in crystalline Si.[107] The quite high formation energies of interstitial B configurations ruled out the "stand-alone" B migration in favor of the BI^0 or BI^+ diffusing pairs. The energy barrier to the diffusion through B*I* pairs is calculated to be 4.5 eV, well in agreement with the experimental determination of Uppal,[104] while the temperature dependence of λ resulted to be almost absent. The activation energy of λ is the difference between the migration and the dissociation energies of the mobile B*I* pair, which are computed to be very similar (both around 1 eV). Later on, Janke and co-workers, by means of *ab-initio* methods, examined the kinetics of boron diffusion, considering a variety of mechanisms (vacancy- or interstitial-mediated, and correlated exchange mechanisms).[106] They also concluded that B diffusion should occur through an *I*-mediated mechanism leading to a B*I* pair in the neutral or positive charge states. Still, the total energy barrier to diffusion is calculated to be 3.8 eV, similar to those found for B diffusion in Si. The discrepancy with the experimental energy barrier determined in Ref. 104 has been attributed to electronic thermal excitations not included in the $T = 0$ K atomistic model.

Still, while calculations of energetics and migration pathways had already suggested reasonable microscopic mechanism of B diffusion through self-interstitials, only recently the experimental validations came out.[108–110] By

comparing the diffusion of Ge, B and P under proton irradiation, Bracht and co-workers demonstrated that *I*-mediated diffusion (as in the B case) is favored under irradiation.[109] The key role of *I*s in B migration was also clearly shown through an independent approach, by investigating the diffusion of B under out of equilibrium conditions for point defect density,[108,110] as described in Sec IV B. In fact, as B is such a slow diffuser, the first experimental studies of its migration mechanism were been limited to a restricted range of very high temperatures and very long times. Hence, alternative methodologies have been used to clarify the B diffusion process in Ge and how point defects can affect B diffusion itself, as detailed in Sec. IV B.

B. Out of equilibrium approach for B migration study

In Si, significant insights on the diffusion mechanisms of dopants came from studies involving out of equilibrium concentrations of point defects induced by ion implantation.[4,65] Typically, ion implantation in Ge hardly comes up with the formation of stable *I*-type defects. Only recently, it has been clarified that end-of-range (EOR) extended defects do also form in Ge after pre-amorphization followed by SPE regrowth,[111,112] even if defects are much smaller and less stable than in Si. Still, as in Si, they are made up of *Is* and their thermal dissolution was shown to induce TED of B.[110] In this case, EOR defects were formed by self-amorphization close to a B delta, whose broadening was measured at temperatures between 300 and 550 °C by SIMS profiling. After B diffusion simulation (based on the same g-λ diffusion model used for B in Si, as explained hereafter), the total number of diffusion events gt was measured and plotted versus temperature together with the EOR induced strain integral measured by high-resolution X-ray diffraction (HRXRD) (Fig. 19). The strain integral can be considered as a quantitative estimation of *Is* contained in the EOR defects,[113] so the Arrhenius plot shows that the more *Is* are released from the EOR (the strain integral decreases), the higher is the number of diffusion events recorded. This strong correlation directly evidences that the diffusion of B atoms is assisted by *Is*. In addition, it shows that the dissolution of EOR occurs in the 350-420 °C temperature range. The energy barrier to EOR thermal dissolution (∼2.1 eV) resulted significantly lower than that (3.8 eV) found for the dissolution of {311} defects in Si, which is consistent with the lower strength of the Ge-Ge bond with respect to the Si-Si bond and with the observation that EOR defects in Ge are weaker and smaller than in Si.

A significantly greater enhancement of B diffusivity over a wider temperature range came out by an alternative approach we developed to allow a much more detailed investigation of the B diffusion mechanism. The method consists in monitoring the broadening of a B delta (grown by MBE) during irradiation with light ions at different target temperatures.[108] By this way, we demonstrated the occurrence of radiation enhanced diffusion (RED) of B in Ge, several orders of magnitude larger than under equilibrium conditions. Some years ago, RED of B in Ge was actually proposed by Uppal and coworkers to explain the long tails occurring after B implantation in Ge at low energy, even if no further investigation was given.[17,114] In Fig. 20, the broadening of a B delta can be seen after H^+ or O^+ irradiation (with fluences well below the amorphization threshold) performed at 150 °C, compared with the negligible thermal diffusion (TD) (at an higher temperature, 350 °C, and for the longest implant time). Boron RED is certainly not due to a direct knock-on phenomenon on B atoms generated by the impinging ion beam (displaced B atoms are actually a negligible fraction of the diffusing B). Thus, the B diffusion observed in Fig. 20 can be related to the interaction of B with the point defects (PDs) or with the free carriers generated by the implantation.

To disentangle the effect of point defect generation from the ionization, we compared (Fig. 20) B diffusion after implantation of H^+ or O^+ ions (with different energies so to have the same projected range, R_p, of ∼2.5 μm). Oxygen has a mass 16 times higher than hydrogen, producing denser

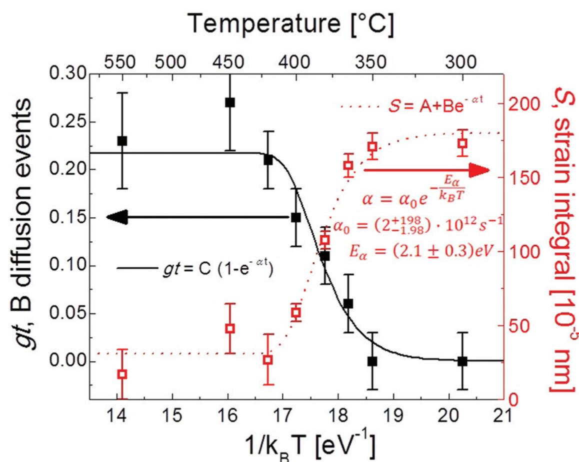

FIG. 19. B diffusion induced by dissolution of EOR defects. The average number of B diffusion events (gt, closed squares, left axis) and the EOR strain integral (S, open squares, right axis) are reported into an Arrhenius plot. The lines are fit to the data considering the exponential functions reported into the graph (parameters A, B, and C account for the initial and saturation values).

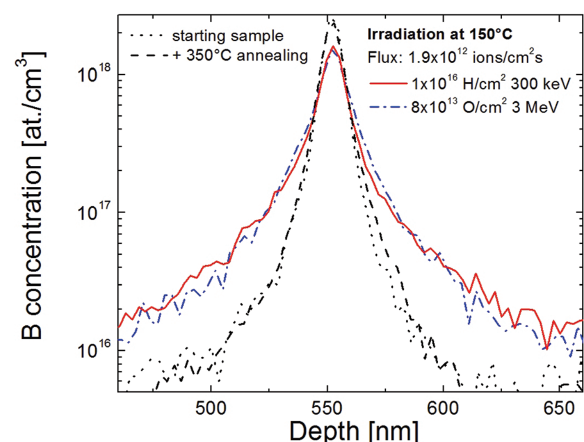

FIG. 20. Ion irradiation effects on the chemical profiles of B in Ge. Starting sample (i.e., the as-grown sample after the 1 h 600 °C annealing, dotted line) and those further irradiated at 150 °C with the 300 keV, 1 × 10^{16} H^+/cm^2 (continuous line) or 3 MeV, 8 × 10^{13} O^+/cm^2 (dashed-dotted line) are reported, together with a non-implanted sample thermally annealed at 350 °C for the longer implant time (dashed line).

collision cascades, so the O^+ fluence was chosen in order to produce the same total energy loss by nuclear collisions as for the H^+ implant in the B-delta region.[115] This leads to a similar generation of PDs, which potentially can interact with B before their recombination. On the other hand, the ratio of the energy lost by interaction with electrons $(dE/dx)_e$ to that lost through elastic collisions with target ions $(dE/dx)_n$, as calculated by the TRIM code,[115] is 10 times larger for the H^+ irradiation than in the O^+ case. We can then distinguish if PDs or ionization affect RED.[116] Fig. 20 shows that the B diffusion is very similar in the two cases, suggesting that indeed the process is mainly driven by the energy deposited into nuclear elastic collisions, producing point-defects, while ionization effects are negligible, if any. This was also confirmed by the evidence that B undergoes an enhanced diffusion also after ion irradiation,[108] as in this last case, ionization effects are truly absent.

Once stated that B diffusion is activated by *I*s, as those produced during ion irradiation,[108,109] the thermal behavior was studied. In Fig. 21, the diffused B profiles under proton irradiation are plotted for different target temperatures, together with the starting B profile and that annealed at 800 °C for the same time but without implantation (i.e., the TD blue open circles). For all the temperatures, under proton irradiation a significant B broadening is observed, much larger than what obtained at 800 °C in equilibrium conditions. Also at RT, some B diffusion can be appreciated (not shown) while, if the B delta is irradiated at the liquid nitrogen temperature,

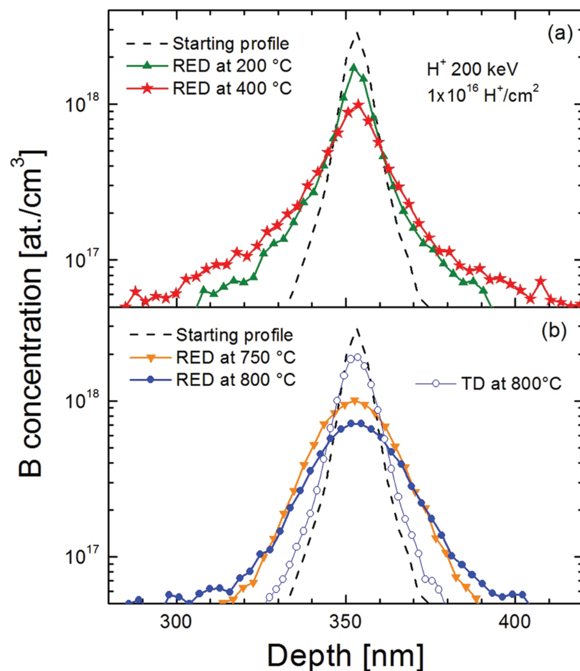

FIG. 21. Temperature effect on the shape of diffused B profile: lower temperatures (upper panel) lead to long exponential tails because of the long migration length. Chemical B profile in the starting sample (dashed line) and after 200 keV H^+ implant performed at 200 °C (upper panel, line plus up triangles), 400 °C (upper panel, line plus stars), 750 °C (lower panel, line plus down triangles), and 800 °C (lower panel, line plus diamonds). A reference for thermal diffusion at 800 °C is also plotted in panel (b) (line plus open circles). Reprinted from G. G. Scapellato *et al.*, Nucl. Instrum. Methods Phys. Res. B **282**, 811 (2012). Copyright (2012) Elsevier.

no diffusion is observed, meaning that the ion-assisted diffusion needs to be thermally activated.[108] Then, the very low B diffusivity under equilibrium conditions can be imputed to the intrinsic lack of self-interstitial defects in Ge, while if *Is* are supplied (as during implantation) B migration occurs, also up to great extents.

A careful look of Fig. 21 also reveals that the shapes of the B diffused profiles change between panels (a) and (b). In the upper panel, the shape of B diffused profiles shows very long exponential tails typical of a long migration path in a diffusion mediated by point defects.[1] On the other hand, the profiles at 750 °C and 800 °C (lower panel) show a Gaussian shape, revealing a shorter diffusion path. Moreover, the lower concentration peak at higher temperatures ($\sim$7.1 $\times 10^{17}$/cm^3 at 800 °C, while $\sim$1.7 $\times$ 10^{18}/cm^3 at 200 °C) indicates a higher number of diffusion events if the temperature increases. All these features appear really akin to what observed by Cowern and co-workers when studying the mechanism of B diffusion in Si,[1,56] thus boron RED phenomena in Ge were studied by fitting all the B profiles with a g-λ diffusion model[108] for B as done for the Si matrix [Sec. III]. Once more, the model assumes that a substitutional B atom (B_s) becomes mobile (B_m) with a rate g by interacting with PDs and then B_m moves for a mean length (λ) before returning substitutional, i.e., immobile. Within this model, we cannot distinguish if the mobile B is an interstitial B (pure kick-out diffusion) or a B*I* pair (interstitialcy diffusion), since the diffused profile is insensitive to the mobile species. As above outlined, theoretical calculations lean toward the interstitialcy diffusion mechanism, but here we will refer to B_m as mobile B (either species). The simulation profiles (not shown here) well agree with the experimental data, as shown in Refs. 108, 110, and 117.

Simulation results indicate that the migration rate (g) is proportional to the ion flux but independent of the ion fluence, while the total number (gt) of migration events per B atom only depends on the ion fluence, being unaffected by the ion flux (within the investigated ranges). This points out that B migration can be switched on and regulated by the implant parameters through the production of self-interstitials defects.[108] The migration path (λ) of B_m is unaffected by both the ion flux and fluence, being dependent only on the irradiation temperature (Fig. 22). Once B diffusion has started, the ion irradiation has no more significant effect on the migrating species, which moves for a length limited by recombination (B_m becomes substitutional) or impurity trapping.[108]

In Fig. 22 all the λ values extracted by simulations under thermal or enhanced conditions for B diffusion in Ge are plotted from 150 to 800 °C.[108,116,118] Migration values are reported for B diffusion during irradiation at different temperatures (RED: 200 keV H^+, or 300 keV H^+, or O^+ irradiation), for annealing after irradiation (300 keV H^+, done at room temperature), and for thermal diffusion. Regardless of diffusion conditions, reported data indicate a migration length smaller than 10 nm for temperatures higher than $\sim$600 °C and a saturation behavior for lower temperatures. In Si, λ has a negative activation energy (~-0.6 eV,[14,56]) as a consequence of the competition between migration and

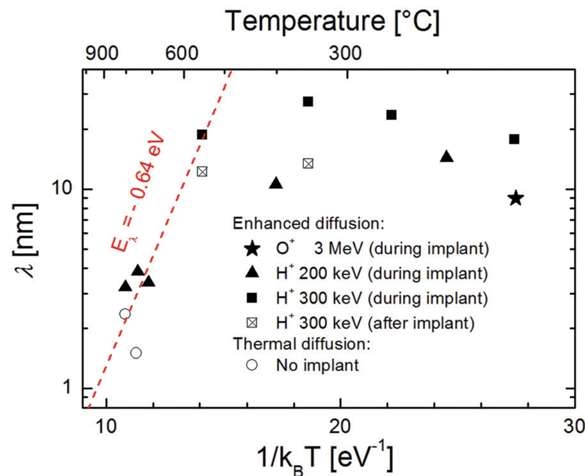

FIG. 22. Arrhenius plot of the diffusion length (λ) for B diffusion in Ge, under several conditions. Enhanced diffusion conditions are reported for samples irradiated at different temperatures with 3 MeV O^+ (star), or with 200 keV H^+ (triangles), or with 300 keV H^+ (squares), and also for samples annealed after 300 keV H^+ irradiation at room temperature (crossed squares). Thermal conditions are also reported for annealing (with no implantation) at 755 °C and 800 °C (open circles). Dashed red line is a fit of λ values obtained in high temperature regime (550-800 °C).

dissociation of the mobile species, thus the migration length reduces by increasing the temperature. In Fig. 22, we observe this trend in the 800-550 °C range, both for RED and TD, confirming that the mobile species B_m stops its diffusion through a thermally activated dissociation process, with an energy barrier of −0.64 eV. Although this evidence is in contrast with the athermal dependence of the migration length predicted in Ref. 107, the similarity between the activation energy of λ in Si and Ge suggests that the migrating species behaves in the same way, at least in terms of diffusivity and dissociation energetics. At lower temperature, the λ trend in Fig. 22 is fairly constant at 10-20 nm, probably because the migration path of mobile B is limited by traps present in the sample (as O or C incorporated during the MBE growth).[108]

The out of equilibrium approach allowed a deep experimental investigation of the B diffusion in Ge, also opening a route for the discovery of new classes of native point defects in crystalline materials.[15] Here, wide similarities between B diffusion mechanisms in Si and Ge have been evidenced, as the same key role of *Is* in activating the migration process and the similar temperature dependence of the migration length. Thus, the depressed diffusivity in Ge has been ascribed to the intrinsic lack of *Is* defects. As in Si, to control the dopant diffusion, a proper point defect engineering should be pursued, as outlined in Sec. IV C.

C. Point defect engineering and enhanced B diffusion

Differently from Si, crystalline Ge has a quite low *Is* density under equilibrium conditions, thus the role of *Is* results to be quite small, not only for dopant diffusion but also for extended defects formation. In Sec. IV B, EOR defects in Ge are shown to be weaker and smaller than in Si, thus a different approach should be conceived to realize a well-built *Is* source in Ge. In fact, the diffusion and deactivation of many dopant atoms in Ge are dominated by vacancies, therefore a proper engineering of point defect density could open the route for innovative frameworks for Ge. In the following, we will show a technique, based on oxygen implantation, able to modify the equilibrium balance of point defects in Ge in favor of self-interstitials and then able to greatly enhance B diffusion.

In Si, a self-interstitial supersaturation is typically produced during surface oxidation because of the different densities of Si and SiO_2.[119] The consequent stress at the Si/SiO_2 interface is partially released by injecting self-interstitials in the bulk, responsible for the oxidation enhanced diffusion (OED) of B. The same approach in Ge is not effective due to GeO desorption at the surface, which leads to unstable Ge oxide.[120,121] Still, if Ge oxidation is forced far away from the surface, some *Is* injection can be obtained. Actually, very recently, it was shown that O implantation in Ge followed by 650 °C annealing induces the formation of embedded GeO_2 nanoclusters (5-10 nm in size) able to induce a large TED of B.[117] It should be noted that the observed GeO_2 nanoclusters exhibit a thermal stability considerably much larger than the EOR defects in Ge discussed above. A band of *I*-rich defects was observed by TEM at a depth of ~350 nm, close to the projected range of O implantation. When O implantation and annealing are performed in a MBE grown Ge film containing 5 narrow B deltas (spaced 200 nm each other), a large broadening of B profiles is observed already after 30 min annealing and lasting up to 2 h (Fig. 23). It is straightforward to realize that the equilibrium diffusion of B in Ge at these temperatures and times is negligible at all, and then a large *Is* supersaturation should exist leading to the observed boron TED. Concomitant to the boron TED, a peculiar shape transformation of the oxide nanoclusters from elongated to spherical form is observed up to 2 h annealing, pointing out a strong correlation between the evolution of the GeO_2 nanoclusters and the self-interstitial supersaturation. The embedded GeO_2 nanoclusters act as the self-interstitial source, in a way similar to what occurs at the surface in Si OED.[117] Still, when the embedded GeO_2 nanoclusters are involved a much

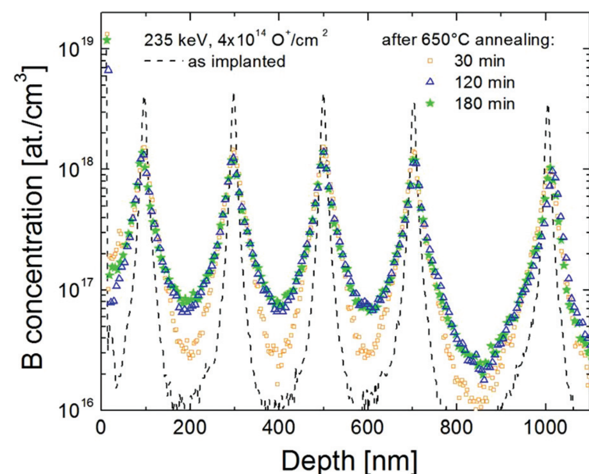

FIG. 23. Effect of embedded GeO_2 nanoclusters on B diffusion in Ge. Boron profiles in MBE-Ge sample after O implantation (black dashed line), and after annealing at 650 °C for 30 (orange open squares), 120 (blue open triangles), and 180 (green stars) min. A homogeneous broadening of the B profiles is observed, evidencing at 650 °C a transient enhanced diffusion of B lasting up to 120 min. Reprinted from G. G. Scapellato, Phys. Rev. B **84**, 024104 (2011). Copyright (2011) The American Physical Society.

larger enhancement of B diffusivity is reached (10^5 for B in Ge against 10 times for OED in Si[122]), due on one side to the very low equilibrium *Is* density in Ge, and on the other side to the very effective self-interstitial injection by the GeO_2 nanoclusters. In fact, based on the different Ge densities in Ge or in GeO_2 (4.8 or 2.4×10^{22} Ge/cm^3, respectively), the volume per Ge atom in the oxide is twice than in bulk, and the stress at the nanocluster surface can be released by injecting self-interstitials in the surrounding lattice. Fig. 23 also shows that B delta diffusion occurs all over the Ge film thickness ($\sim$1 μm) even if the GeO_2 nanoclusters are located at a depth of $\sim$350 nm below the surface. As *I*s are injected by the GeO_2 nanoclusters and diffusion of B delta is observed up to a depth of 1000 nm (deepest B δ in Fig. 23) just after 30 min at 650 °C, one can evaluate $\sim 2 \times 10^{-12}$ cm^2/s as a lower estimate for *I* diffusivity in Ge at 650 °C. This datum shows that, once formed, self-interstitials can affect the Ge lattice at long distances and in a non-negligible way, remarking that the weak role of self-interstitials in Ge is related to their scarcity in equilibrium conditions.

By summarizing, the ion irradiation approach allowed the experimental investigation of B diffusion in Ge confirming the theoretical prediction of an *I*-mediated mechanism. Some similarities between B migration in Ge and Si can be drawn, as the mechanism itself and the energetics of the migrating species (activation energy for λ), still the main difference is the much lower B diffusivity in Ge clearly due to the intrinsic shortage of self-interstitial defects. When *Is* are supplied, large B diffusion is observed also at relatively low temperatures. Point defects engineering methods for stable *Is* sources are investigated, showing that the formation of embedded GeO_2 nanoclusters is the most promising way to sustain a large *Is* supersaturation at 650 °C. A proper modification of the equilibrium *I-V* density, naturally overbalanced towards *V*s, can be beneficial for a variety of phenomena detrimentally affected by *V*s in Ge as the enhanced diffusion or the deactivation of most dopants.

V. CONCLUSIONS

In this paper, we reviewed the key features of B migration in different matrices, such as amorphous (α) or crystalline (c) Si or Ge. The underlying microscopic mechanisms have been investigated and modeled, showing that in all the cases, the dopant diffusion is always an indirect process.

In α-Si, B diffusivity is well larger (a factor of 10^5) than in c-Si, causing a non negligible broadening of the dopant profile and a very quick precipitation when B is implanted in pre-amorphized silicon during ultra-shallow junction fabrication. We showed that B migration in α-Si is activated by dangling bonds of the amorphous structure, being these defects enhanced in density by the B itself. Such a feature induces the peculiar shape of the diffused profile, where the concentration gradient unexpectedly increases after diffusion, since the higher the B density, the more dangling bonds are present, promoting a more effective B migration. Because of this apparent violation of the Fick's law, we developed a proper model considering the interplay between dopant atoms and point defects, and able to accurately simulate the B diffusion in α-Si, also accounting for the quick dopant precipitation above 2×10^{20} B/cm^3. The diffusivity coefficients for boron and dangling bonds have been measured, showing Arrhenius behaviors over five orders of magnitude, with relative energy barriers of 3.0 and 2.6 eV, respectively. The proposed model was shown to be able to simulate B diffusion in α-Si, also under typical conditions used for ultra-shallow junction realization. Basing on the revealed strong interplay between B and point defects in the amorphous structure of Si, similar behavior is expected for other dopants, which are three- or five-fold coordinated in Si and could show diffusion in α-Si with features similar to those already modeled for B.

In c-Si, the microscopic pathways of B migration and the diffusivity values significantly change depending on the Fermi level position. In fact, B diffusion takes place through an interstitialcy mechanism, under intrinsic conditions involving neutral self-interstitials (I^0), while under extrinsic conditions (*p*-type doping), the interaction of substitutional B (B_S^-) with doubly positively charged selfinterstitials (I^{++}) is more and more probable, leading to enhanced dopant diffusivity. In both the cases, a charge exchange with the surrounding matrix occurs giving the neutral BI^0 pair, which is the migrating species. Instead, under high *n*-type doping conditions, a depression of diffusivity is observed, with non negligible contribution to B diffusion given by the negatively charged B*I* complex and by Coulomb pairing effects of B with *n*-type dopants (more effective with P than with As). In any cases, B diffusion in c-Si is also heavily affected by non-equilibrium clustering with *Is*. In fact, the temporary immobilization of B into BICs alters both the density of diffusing boron atoms and that of self-interstitials, needed to start the B diffusion itself. In addition, BICs also affect the electrical behavior because of B de-activation and charge carrier mobility degradation. Under prolonged annealing, these BICs dissolve releasing both B and *Is* and, thus, influencing B migration. BICs are usually very small (below 1 nm in size) and dissolve with an energy barrier of 3.6 eV; nonetheless quite large (5-10 nm in size) BICs, dissolving with a larger barrier (4.8 eV), can be formed under conditions of very high B concentrations and moderate *Is* supersaturation. In fact, beyond the above two main families, a more complex interplay occurs between BICs with different size and thermal stability, which has been recently approached by an appropriate model based on atomistic calculations.

In Ge, the mechanism of B diffusion has been studied to a lower extent than in Si, and essentially limited to the crystalline Ge case. Nevertheless, it is now clear that the dopant migration mechanism is assisted by Ge self-interstitial too, repeating what occurs in c-Si. The boron diffusivity values in Ge are much smaller than in Si (up to five orders of magnitude), while the activation barrier is well larger (4.65 eV rather than 3.45 eV). These features can be explained within the model of B migration assisted by self-interstitials, because of the intrinsic shortage of self-interstitials in Ge lattice and of their large formation energy. In fact, we show that if self-interstitials are furnished out-of equilibrium (as during ion irradiation experiments), B diffusion occurs up to quite large extents and also at relatively low temperatures. Moreover, B diffused profiles have been satisfactorily fitted

with the same model of B diffusion used for Si. In addition, we showed that if a proper point defects modification is reached, as after O implant, which creates an effective source for *Is*, B diffusion can be strongly enhanced over large distances. Further aspects to be investigated are the mechanism of B diffusion in Ge under extrinsic conditions, and the pairing with other dopants, if any. The peculiarity of the very low *Is* density in Ge, and the evidence for *Is* need in boron migration, makes the B diffusion in Ge a really intriguing phenomenon, required to be further investigated.

Finally, whatever the matrix is, B migration in α-Si, c-Si, or c-Ge, is shown to be an indirect phenomenon occurring by means of interaction with point defects of the hosting lattice, specifically self-interstitials, or dangling bonds, if in crystalline or in amorphous materials, respectively. Because of this, any modeling of B diffusion has to take into great account the density and diffusivity of the specific point defect acting as the mediator.

ACKNOWLEDGMENTS

The authors express their gratitude to J. M. Poate and E. Rimini, for encouraging them in writing this review, and acknowledge the relevant contributions given to the research work by G. Bisognin, S. Boninelli, A. Carnera, G. Impellizzeri, M. Mastromatteo, E. F. Pecora, C. Percolla, G. G. Scapellato, R. Storti, S. Tatì, and A. Terrasi.

[1]N. E. B. Cowern, K. T. F. Janssen, G. F. A. van de Walle, and D. J. Gravesteijn, Phys. Rev. Lett. **65**, 2434 (1990).
[2]B. Sadigh, T. J. Lenosky, S. K. Theiss, M.-J. Caturla, T. Diaz de la Rubia, and M. A. Foad, Phys. Rev. Lett. **83**, 4341 (1999).
[3]W. Windl, M. M. Bunea, R. Stumpf, S. T. Dunham, and M. P. Masquelier, Phys. Rev. Lett. **83**, 4345 (1999).
[4]P. A. Stolk, H.-J. Gossmann, D. J. Eaglesham, D. C. Jacobson, C. S. Rafferty, G. H. Gilmer, M. Jaraiz, J. M. Poate, H. S. Luftman, and T. E. Haynes, J. Appl. Phys. **81**, 6031 (1997).
[5]See www.itrs.net for future technology requirements of the semiconductor industry.
[6]F. Severac, F. Cristiano, E. Bedel-Pereira, P. F. Fazzini, J. Boucher, W. Lerch, and S. Hamm, J. Appl. Phys. **107**, 123711 (2010).
[7]W. Lerch, S. Paul, J. Niess, S. McCoy, J. Gelpey, F. Cristiano, F. Severac, P. Fazzini, A. Martinez-Limia, P. Pichler, H. Kheyrandish, and D. Bolze, Mater. Sci. Eng. B **154-155**, 3 (2008).
[8]B. J. Pawlak, W. Vandervorst, A. J. Smith, N. E. B. Cowern, B. Colombeau, and X. Pages, Appl. Phys. Lett. **86**, 101913 (2005).
[9]K. Sekar, W. Krull, K. Huet, C. Boniface, and J. Venturini, AIP Conf. Proc. **1321**, 101–104 (2011).
[10]V. C. Venezia *et al.*, Mater. Sci. Eng. B **124-125**, 245 (2005).
[11]S. Mirabella *et al.*, Phys. Rev. Lett. **100**, 155901 (2008).
[12]A. Mattoni and L. Colombo, Phys. Rev. B **69**, 045204 (2004).
[13]D. De Salvador, G. Bisognin, M. Di Marino, E. Napolitani, A. Carnera, H. Graoui, M. A. Foad, F. Boscherini, and S. Mirabella, Appl. Phys. Lett. **89**, 241901 (2006).
[14]D. De Salvador, E. Napolitani, G. Bisognin, M. Pesce, A. Carnera, E. Bruno, G. Impellizzeri, and S. Mirabella, Phys. Rev. B **81**, 045209 (2010).
[15]N. E. B. Cowern *et al.*, arXiv:1210.2902v2 (2012).
[16]C. Claeys and E. Simoen, *Germanium-Based Technologies—From Materials to Devices* (Elsevier, Amsterdam, 2007).
[17]S. Uppal *et al.*, J. Appl. Phys. **90**, 4293 (2001).
[18]H. Bracht and S. Brotzmann, Mater. Sci. Semicond. Process. **9**, 471 (2006) and references therein.
[19]S. Mirabella *et al.*, Appl. Phys. Lett. **92**, 251909 (2008).
[20]P. A. Stolk *et al.*, J. Appl. Phys. **75**, 7266 (1994) and references therein.
[21]L. Pelaz *et al.*, J. Appl. Phys. **96**, 5947 (2004) and references therein.
[22]S. T. Pantelides, Phys. Rev. Lett. **57**, 2979 (1986).
[23]P. C. Kelires and J. Tersoff, Phys. Rev. Lett. **61**, 562 (1988).
[24]R. Biswas *et al.*, Phys. Rev. Lett. **63**, 1491 (1989).
[25]M. Stutzmann and D. K. Biegelsen, Phys. Rev. B **40**, 9834 (1989).
[26]S. Roorda, S. Doorn, W. C. Sinke, P. M. L. O. Scholte, and E. vanLoenen, Phys. Rev. Lett. **62**, 1880 (1989).
[27]S. Roorda *et al.*, Phys. Rev. B **44**, 3702 (1991).
[28]K. Laaziri *et al.*, Phys. Rev. Lett. **82**, 3460 (1999).
[29]J. M. Poate *et al.*, Nucl. Instrum. Methods Phys. Res. B **19/20**, 480 (1987).
[30]A. Polman *et al.*, Appl. Phys. Lett. **57**, 1230 (1990).
[31]S. Coffa *et al.*, Phys. Rev. B **45**, 8355 (1992).
[32]I. Santos *et al.*, Phys. Rev. B **83**, 153201 (2011).
[33]R. Duffy *et al.*, Appl. Phys. Lett. **84**, 4283 (2004).
[34]G. N. Graves *et al.*, Phys. Rev. B **45**, 6517 (1992).
[35]G. N. Graves *et al.*, Nucl. Instrum. Methods Phys. Res. B **80/81**, 966 (1993).
[36]G. Muller *et al.*, Philos. Mag. B **69**, 177 (1994).
[37]G. Muller *et al.*, Philos. Mag. B **73**, 245 (1996).
[38]G. Muller, Curr. Opin. Solid State Mater. Sci. **3**, 364 (1998).
[39]J. M. Jacques *et al.*, Appl. Phys. Lett. **82**, 3469 (2003).
[40]P. M. Fahey, P. B. Griffin, and J. D. Plummer, Rev. Mod. Phys. **61**, 289 (1989).
[41]S. M. Myers and D. M. Follstaedt, J. Appl. Phys. **79**, 1337 (1996).
[42]N. Bernstein, J. L. Feldman, and M. Fornari, Phys. Rev. B **74**, 205202 (2006).
[43]I. Martin-Bragado and N. Zographos, Solid-State Electron. **55**, 25 (2011).
[44]R. B. Fair and P. N. Pappas, J. Electrochem. Soc. **122**, 1241 (1975).
[45]S. M. Hu, J. Appl. Phys. **45**, 1567 (1974).
[46]D. A. Antoniadis and I. Moskowitz, J. Appl. Phys. **53**, 6788 (1982).
[47]U. Goesele and T. Y. Tan, in *Defects in Semiconductors II*, edited by S. Mahajan and J. W. Corbett (North-Holland, New York, 1983), p. 45.
[48]T. Y. Tan and U. Goesele, Appl. Phys. A **37**, 1 (1985).
[49]H.-J. Gossmann, T. E. Haynes, P. A. Stolk, D. C. Jacobson, G. H. Gilmer, J. M. Poate, H. S. Luftam, T. K. Mogi, and M. O. Thompson, Appl. Phys. Lett. **71**, 3862 (1997).
[50]A. Ural, P. B. Griffin, and J. D. Plummer, Appl. Phys. Lett. **73**, 1706 (1998).
[51]U. Gösele, P. Laveant, R. Scholz, N. Engler, and P. Werner, in *Si Front-End Processing-Physics and Technology of Dopant-Defect Interactions II*, Mater. Res. Soc. Symp. Proc. Vol. 610, edited by A. Agarwal *et al.* (Material Research Society, Warrendale, 2000).
[52]C. S. Nichols, C. G. Van de Walle, and S. T. Pantelides, Phys. Rev. Lett. **62**, 1049 (1989).
[53]J. Zhu, T. Diaz de la Rubia, L. H. Yang, C. Mailhiot, and G. H. Gilmer, Phys. Rev. B **54**, 4741 (1996).
[54]P. Alippi, L. Colombo, P. Ruggerone, A. Sieck, G. Seifert, and Th. Frauenheim, Phys. Rev. B **64**, 075207 (2001).
[55]I. Martin-Bragado, P. Castrillo, M. Jaraiz, R. Pinacho, J. E. Rubio, and J. Barbolla, Phys. Rev. B **72**, 35202 (2005).
[56]N. E. B. Cowern, G. F. A. van de Walle, D. J. Gravesteijn, and C. J. Vriezema, Phys. Rev. Lett. **67**, 212 (1991).
[57]M. D. Giles, J. Electrochem. Soc. **138**, 1160 (1991).
[58]D. J. Eaglesham, P. A. Stolk, H.-J. Gossmann, T. E. Haynes, and J. M. Poate, Nucl. Instrum. Methods B **106**, 1919 (1995).
[59]M. E. Law, G. H. Gilmer, and M. Jaraìz, Mater. Res. Soc. Bull. **25**, 45 (2000).
[60]W. K. Hofker, H. W. Werner, D. P. Oosthoek, and H. A. M. de-Grefte, Appl. Phys. **2**, 165 (1973).
[61]W. K. Hofker, H. W. Werner, D. P. Oosthoek, and N. J. Cowman, Appl. Phys. **4**, 125 (1974).
[62]A. E. Michel, W. Rausch, P. A. Ronsheim, and R. H. Kasti, Appl. Phys. Lett. **50**, 416 (1987).
[63]N. E. B. Cowern, G. F. A. Van de Walle, P. C. Zalm, and D. W. E. Vandenhoudt, Appl. Phys. Lett. **65**, 2981 (1994).
[64]D. J. Eaglesham, P. A. Stolk, H. J. Gossmann, and J. M. Poate, Appl. Phys. Lett. **65**, 2305 (1994).
[65]S. C. Jain, W. Schoenmaker, R. Lindsay, P. A. Stolk, S. Decoutere, M. Willander, and H. E. Maes, J. Appl. Phys. **91**, 8919 (2002).
[66]D. De Salvador, E. Napolitani, S. Mirabella, G. Bisognin, G. Impellizzeri, A. Carnera, and F. Priolo, Phys. Rev. Lett. **97**, 255902 (2006).
[67]E. Napolitani, D. De Salvador, R. Storti, A. Carnera, S. Mirabella, and F. Priolo, Phys. Rev. Lett. **93**, 055901 (2004).
[68]E. Napolitani, D. De Salvador, M. Pesce, A. Carnera, S. Mirabella, and F. Priolo, J. Vac. Sci. Technol. B **24**, 394 (2006).

[69]P. Pichler, *Intrinsic Point Defects, Impurities, and Their Diffusion in Silicon*, edited by S. Selberherr (Springer, NewYork, 2004).
[70]H. Bracht, H. H. Silvestri, I. D. Sharp, and E. E. Haller, Phys. Rev. B **75**, 035211 (2007) and references therein.
[71]W. Windl, Appl. Phys. Lett. **98**, 202104 (2008).
[72]S. Solmi, F. Baruffaldi, and R. Canteri, J. Appl. Phys. **69**, 2135 (1991).
[73]N. E. B. Cowern, K. T. F. Janssen, H. F. F. Jobs, J. Appl. Phys. **66**, 6191 (1990).
[74]N. E. B. Cowern, A. Cacciato, J. S. Custer, F. W. Saris, and W. Vanderwost, Appl. Phys. Lett. **68**, 1150 (1996).
[75]T. E. Haynes, D. J. Eaglesham, P. A. Stolk, H.-J. Gossmann, D. C. Jacobson, and J. M. Poate, Appl. Phys. Lett. **69**, 1376 (1996).
[76]M. B. Huang and I. V. Mitchell, J. Appl. Phys. **85**, 174 (1999).
[77]G. Mannino, N. E. B. Cowern, F. Roozeboom, and J. G. M. Van Berkum, Appl. Phys. Lett. **76**, 855 (2000).
[78]S. Solmi, M. Bersani, M. Sbetti, J. Lundsgaard Hansen, and A. Nylandsted Larsen, J. Appl. Phys. **88**, 4547 (2000).
[79]L. Pelaz, M. Jaraiz, G. H. Gilmer, H.-J. Gossmann, C. S. Rafferty, D. J. Eaglesham, and J. M. Poate, Appl. Phys. Lett. **70**, 2285 (1997).
[80]L. Pelaz, G. H. Gilmer, H.-J. Gossmann, C. S. Rafferty, M. Jaraiz, and J. Barbolla, Appl. Phys. Lett. **74**, 3657 (1999).
[81]W. Luo, P. B. Rasband, P. Clancy, and B. W. Roberts, J. Appl. Phys. **84**, 2476 (1998).
[82]M. J. Caturla, M. D. Johnson, and T. D. de la Rubia, Appl. Phys. Lett. **72**, 2736 (1998).
[83]X.-Y. Liu, W. Windl, and M. P. Masquelier, Appl. Phys. Lett. **77**, 2018 (2000).
[84]T. J. Lenosky, B. Sadigh, S. K. Theiss, M. J. Caturla, and T. D. de la Rubia, Appl. Phys. Lett. **77**, 1834 (2000).
[85]W. Luo and P. Clancy, J. Appl. Phys. **89**, 1596 (2001).
[86]S. Chakravarti and S. T. Dunham, J. Appl. Phys. **89**, 3650 (2001).
[87]P. Alippi, P. Ruggerone, and L. Colombo, Phys. Rev. B **69**, 125205 (2004).
[88]M. Cogoni, A. Mattoni, B. P. Uberuaga, A. F. Voter, and L. Colombo Appl. Phys. Lett. **87**, 191912 (2005).
[89]M. Aboy, L. Pelaz, L. A. Marques, P. Lopez, and J. Barbolla, J. Appl. Phys. **97**, 103520 (2005).
[90]F. Cristiano, X. Hebras, N. Cherkashin, A. Claverie, W. Lerch, and S. Paul, Appl. Phys. Lett. **83**, 5407 (2003).
[91]S. Boninelli, S. Mirabella, E. Bruno, F. Priolo, F. Cristiano, A. Claverie, D. De Salvador, G. Bisognin, and E. Napolitani, Appl. Phys. Lett. **91**, 031905 (2007).
[92]E. Bruno, S. Mirabella, G. Impellizzeri, F. Priolo, F. Giannazzo, V. Raineri, E. Napolitani, Appl. Phys. Lett. **87**, 133110 (2005).
[93]A. D. Lilak, M. E. Law, L. Radic, K. S. Jones, and M. Clark, Appl. Phys. Lett. **81**, 2244 (2002).
[94]F. Severac *et al*., J. Appl. Phys. **105**, 043711 (2009).
[95]T. Clarysse, J. Bogdanowicz, J. Goossens, A. Moussa, E. Rosseel, W. Vandervorst, D. H. Petersen, R. Lin, P. F. Nielsen, O. Hansen, G. Merklin, N. S. Bennett, and N. E. B. Cowern, Mater. Sci. Eng. B **154-155**, 24 (2008).
[96]M. Aboy, L. Pelaz, E. Bruno, S. Mirabella, and S. Boninelli, J. Appl. Phys. **110**, 073524 (2011).
[97]S. Mirabella, E. Bruno, F. Priolo, D. De Salvador, E. Napolitani, A. V. Drigo, and A. Carnera, Appl. Phys. Lett. **83**, 680 (2003).
[98]D. De Salvador, E. Napolitani, G. Bisognin, A. Carnera, E. Bruno, S. Mirabella, G. Impellizzeri, F. Priolo, Appl. Phys. Lett. **87**, 221902 (2005).
[99]F. A. Trumbore, Bell Syst. Technol. J. **39**, 205 (1960).
[100]J. Vanhellemont and E. Simoen, J. Electrochem. Soc. **154**, H572 (2007).
[101]A. Satta, E. Simoen, T. Clarisse, T. Janssens, A. Benedetti, B. De Jaeger, M. Meuris, and W. Vandervorst, Appl. Phys. Lett. **87**, 172109 (2005).
[102]Y.-L. Chao, S. Prussin, J. C. S. Woo, and R. Scholz, Appl. Phys. Lett. **87**, 142102 (2005).
[103]L. A. Edelman, M. S. Phen, K. S. Jones, R. G. Elliman, and L. M. Rubin, Appl. Phys. Lett. **92**, 172108 (2008).
[104]S. Uppal *et al*., J. Appl. Phys. **96**, 1376 (2004).
[105]A. Chroneos, B. P. Uberuaga, and R. W. Grimes, J. Appl. Phys. **102**, 083707 (2007).
[106]C. Janke, R. Jones, S. Oberg, and P. R. Briddon, Phys. Rev. B **77**, 075208 (2008).
[107]P. Delugas and V. Fiorentini, Phys. Rev. B **69**, 085203 (2004).
[108]E. Bruno, S. Mirabella, G. G. Scapellato, G. Impellizzeri, A. Terrasi, F. Priolo, E. Napolitani, D. De Salvador, M. Mastromatteo, and A. Carnera, Phys. Rev. B **80**, 033204 (2009).
[109]H. Bracht, S. Schneider, J. N. Klug, C. Y. Liao, J. Lundsgaard Hansen, E. E. Haller, A. Nylandsted Larsen, D. Bougeard, M. Posselt, and C. Wündisch, Phys. Rev. Lett. **103**, 255501 (2009).
[110]E. Napolitani, G. Bisognin, E. Bruno, M. Mastromatteo, G. G. Scapellato, S. Boninelli, D. De Salvador, S. Mirabella, C.Spinella, A. Carnera, and F. Priolo, Appl. Phys. Lett. **96**, 201906 (2010).
[111]S. Koffel, N. Cherkashin, F. Houdellier, M. J. Hytch, G. Benassayag, P. Scheiblin, and A. Claverie, J. Appl. Phys. **105**, 126110 (2009).
[112]G. Bisognin, S. Vangelista, and E. Bruno, Mater. Sci. Eng., B **154-155**, 64 (2008).
[113]S. Decoster and A. Vantomme, J. Phys. D: Appl. Phys. **42**, 165404 (2009).
[114]S. Uppal *et al*., Physica B **308-310**, 525–528 (2001).
[115]J. F. Ziegler, J. P. Biresack, and U. Littmark, *The Stopping and the Range of Ions in Solids* (Pergamon, New York, 1985).
[116]E. Bruno, S. Mirabella, G. G. Scapellato, G. Impellizzeri, A. Terrasi, F. Priolo, E. Napolitani, D. De Salvador, M. Mastromatteo, and A. Carnera, Thin Solid Films **518**, 2386 (2010).
[117]G. G. Scapellato, S. Boninelli, E. Napolitani, E. Bruno, A. J. Smith, S. Mirabella, M. Mastromatteo, D. De Salvador, R. Gwilliam, C. Spinella, A. Carnera, and F. Priolo, Phys. Rev. B **84**, 024104 (2011).
[118]G. G. Scapellato, E. Bruno, A. J. Smith, E. Napolitani, D. De Salvador, S. Mirabella, M. Mastromatteo, A. Carnera, R. Gwilliam, and F. Priolo, Nucl. Instrum. Methods Phys. Res. B **282**, 811 (2012).
[119]H. Kageshima, M. Uematsu, and K. Shiraishi, Microelectron. Eng. **59**, 301 (2001).
[120]A. Molle, Md. N. K. Bhuiyan, G. Tallarida, and M. Fanciulli, Appl. Phys. Lett. **89**, 083504 (2006).
[121]S. K. Wang, K. Kita, C. H. Lee, T. Tabata, T. Nishimura, K. Nagashio, and A. Toriumi, J. Appl. Phys. **108**, 054104 (2010).
[122]N. Cowern and C. Rafferty, Mater. Res. Soc. Bull. **25**, 39 (2000).